Chapter 8
Electronic Properties of Transition Metal-Benzene Sandwich Clusters

Tsugunosuke Masubuchi and Atsushi Nakajima

Abstract Organometallic clusters composed of transition metal atoms and benzene molecules have been topics of great interest from both fundamental and technological points of view. In this chapter, we review the progress in the physical chemistry of transition metal-benzene clusters. The intrinsic properties of transition metal-benzene clusters as a function of cluster size are investigated by gas-phase experiments, often in combination with quantum chemical calculations. In particular, vanadium-benzene clusters denoted V_nBz_m, showing magic numbers at $m = n + 1$, n, and $n - 1$, are characterized to possess multiple-decker sandwich structures, where vanadium atoms and benzene molecules are alternately piled up. Moreover, the discovery of such multiple-decker formation is a cornerstone in bottom-up approaches of molecular magnetism. The interplay of mass spectrometry, laser spectroscopies, and density functional calculations reveals that multiple-decker V_nBz_m clusters exhibit monotonic increase in magnetic moment with the number of layers. Anion photoelectron spectroscopic studies allow direct observations of the geometric and electronic structures of sandwich clusters and their anions. Major progress in this direction includes the recent characterization of tilted multiple-decker sandwich cluster anions composed of manganese atoms and benzene molecules. The sandwich clusters with high-spin characteristics will hopefully be exploited as building blocks in advanced electronic and magnetic nanomaterials via controlled assembly.

T. Masubuchi
Department of Chemistry, Faculty of Science and Technology, Keio University, Kohoku-ku, Yokohama, Japan

State Key Laboratory of Molecular Reaction Dynamics, Dalian Institute of Chemical Physics, Chinese Academy of Sciences, Dalian, China

A. Nakajima (✉)
Department of Chemistry, Faculty of Science and Technology, Keio University, Kohoku-ku, Yokohama, Japan

Keio Institute of Pure and Applied Sciences (KiPAS), Keio University, Kohoku-ku, Yokohama, Japan
e-mail: nakajima@chem.keio.ac.jp

T. Onishi (ed.), *Theoretical Chemistry for Advanced Nanomaterials*,
https://doi.org/10.1007/978-981-15-0006-0_8

Keywords Sandwich complexes · Multiple-decker sandwich clusters · Mass spectrometry · Photoionization spectroscopy · Anion photoelectron spectroscopy · Molecular magnetism

8.1 Introduction

It was 60 years ago that Feynman [1] delivered a famous lecture named "There's Plenty of Room at the Bottom," where he proposed a concept of designing functionalities by taking full advantage of the properties of things on a small scale. In 1962, Kubo [2] theoretically inferred that physicochemical properties of such small materials are different from those in bulk because of discrete energy levels of electrons. Since then, nanoscale materials have been important subjects in both basic and applied sciences. Among them, clusters consisting of up to about 1000 atoms have been extensively studied as they exhibit unexpected geometric and electronic properties that are scaled as a function of cluster size [3].

In recent decades, indeed, metal clusters and molecular clusters have attracted great attention as novel nanoscale materials of finite multifunctional systems. For metal clusters, spectroscopic and theoretic studies have revealed the size-dependent electronic properties of metal-insulator transition [4] and the electron shell structures based on jellium model [3, 5], the latter of which were discussed also from the viewpoint of mimicking shell model of nucleus [5]. As well as physical properties, chemical properties of size-specific reactivity of the metal clusters have been greatly explored as cluster catalysts [6]. On the other hand, molecular clusters have been extensively studied as the aggregates of weak van der Waals forces or hydrogen bond network, revealing microscopic solvation dynamics [7], coexisting phases [8], and electronic evolution of organic semiconductors [9].

However, studies on hybridized clusters between metal atoms and molecules, organometallic clusters, are limited, although organometallic molecular complexes such as an archetypal complex of ferrocene and ligated metal cluster compounds have been well known [10]. In particular, organometallic cluster formation can facilitate to control the dimensionality of the geometric structure through local metal-ligand interaction [11]. Since a low-dimensional structure of organometallic clusters synergistically exploits the chemical and physical features of metal atoms and organic molecules, leading to a dramatic change in their confinement behavior, functional properties such as charge transfer, conductivity, and electron spin arrangement can be designed by selecting an appropriate organic ligand which optimizes the characteristics of the metal atoms.

Sandwich clusters, consisting of metal atoms and planar ring ligands, are typical organometallic clusters, whose metal-ligand interactions are of fundamental interest due to their unique structures and electronic properties [11]. In this chapter, we focus on transition metal-benzene sandwich clusters. Followed by a general introduction on organometallic sandwich compounds, we explain gas-phase synthesis and characterization studies to probe the structures of transition metal-benzene clusters.

These studies are intended to understand how the structures of metal-benzene clusters are governed by the constituent metal atoms or molecules as well as the cluster size. Then, we refer to joint experimental and theoretical studies, including our recent works, for vanadium-benzene and manganese-benzene clusters and their anions. A special emphasis is put on their electronic and magnetic properties, which are characterized and understood from a nanoscopic point of view.

8.2 Preparation and Structures of Transition Metal-Benzene Sandwich Clusters

8.2.1 Early Studies on Sandwich Complexes

The discovery of ferrocene, a typical metallocene consisting of a Fe(II) atom and two cyclopentadienyl (C_5H_5 = Cp) ligands [12], is counted as a milestone in organometallic chemistry. Chemical, magnetic, and X-ray crystallographic characterizations revealed the sandwich structure of ferrocene, where the iron atom is η^5-bound to both the Cp ligands [13–14]. From the viewpoint of molecular orbital theory, the interaction of the Fe atom and the Cp ligands is shown in Fig. 8.1. In the following way, Lauher and Hoffmann [15] described the kinetic and thermodynamic stability of ferrocene. The *p* orbitals of the two Cp ligands produce three sets of approximately degenerate orbitals: a low-lying filled pair of a_{1g} and a_{2u} symmetry, a filled set of e_{1g} and e_{1u} symmetry, and an unoccupied pair of antibonding orbitals of e_{2g} and e_{2u} symmetry. When these orbitals interact with the Fe 3*d* orbitals, the resultant molecular energy levels of ferrocene are understood in terms of symmetry matching. The e_{1g} orbitals of the Cp ligands strongly interact with the Fe $3d_{yz}$ and $3d_{zx}$ orbitals, yielding a pair of bonding and antibonding orbitals, each of which is doubly degenerate. The a_{1g}, a_{2u}, and e_{1u} orbitals could interact but are much less combined with the Fe 4*s* or 4*p* orbitals that are too high in energy. The $3d_z{}^2$, $3d_{xy}$, and $3d_x{}^2{}_{-y}{}^2$ orbitals of the Fe atom thus remain essentially nonbonding. Ferrocene thus fulfills the 18-electron rule by filling its bonding and nonbonding orbitals. In fact, other metallocenes that do not satisfy the 18-electron rule, such as cobaltocene, $CoCp_2$ [16], are basically less stable than ferrocene.

Besides the metallocene family, bis(benzene)chromium, $CrBz_2$ (Bz = C_6H_6) [17], and bis(cyclooctatetraene)uranium, $U(COT)_2$ (COT = C_8H_8), called uranocene [18], are well-known sandwich compounds (Fig. 8.2). Their molecular orbital interactions between the metal and ligands are described in the same manner as that for ferrocene [19–20]. Bis(benzene)vanadium, VBz_2, was also prepared by the similar (Fischer-Hafner) method that was used for $CrBz_2$, but it was much more immediately oxidized in air than $CrBz_2$ [21]. Likewise, sandwich complexes that do not satisfy the 18-electron rule are difficult to be synthesized in the condensed phase. Another interesting derivative is a triple-decker sandwich complex of Ni atoms and Cp ligands, $[Ni_2Cp_3]^+$ (Fig. 8.2) [22]. Chemical synthesis of multiple-decker sandwich compounds, however, often requires appropriate ligands to stabilize such

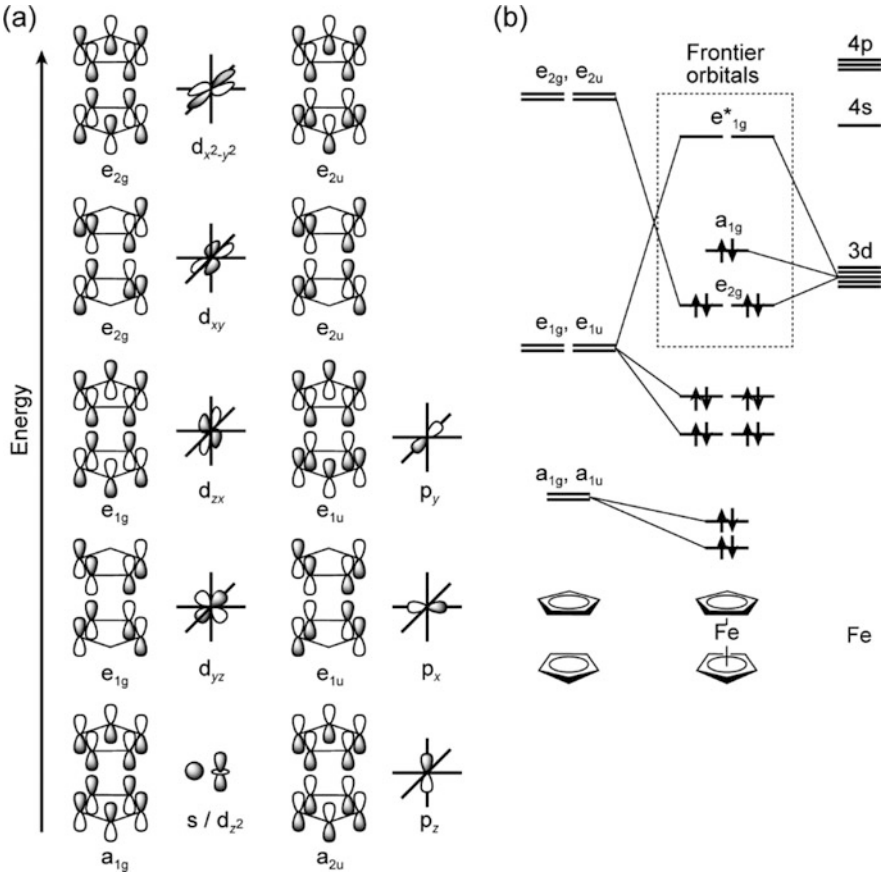

Fig. 8.1 (**a**) Symmetry matching of the molecular orbitals of the Cp ligands with the atomic orbitals of the Fe atom in ferrocene. The e_{2u} orbitals of the Cp ligands do not match with any orbitals of Fe. (**b**) Schematic molecular orbital diagram for ferrocene. The unoccupied e_{*1g} orbitals of ferrocene have antibonding character

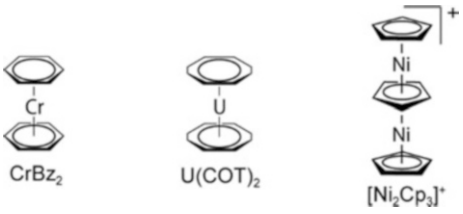

Fig. 8.2 Sandwich structures of $CrBz_2$, $U(COT)_2$, and $[Ni_2Cp_3]^+$

structures, as demonstrated in the early study that yielded up to hexa-decker sandwich complexes by using boron heterocycles instead of Cp [23]. More synthetic attempts on sandwich compounds have been detailed in the former reviews [24–25], and then we do not intend to introduce such contributions in this chapter.

8.2.2 *Gas-Phase Synthesis of Organometallic Complexes*

The development of vacuum techniques has enabled the direct synthesis of difficult-to-form complexes from vaporized materials. Followed by the synthesis of C_3 dicarbene from carbon vapor [27], Timms built the vacuum apparatus depicted in Fig. 8.3 in order to produce a variety of organometallic complexes. In the vacuum apparatus, transition metals were vaporized by the electric heating wire and allowed to react with gaseous organic reagents sprayed from a burette [26, 28]. The early efforts include the synthesis of several sandwich complexes such as bis(benzene)ruthenium, $RuBz_2$ [29], and triple-decker $Cr_2(1,3,5\text{-mesitylene})_3$ [30] in this way. In these studies, NMR spectroscopy was used for the structural characterization. Importantly, this gas-phase synthesis of sandwich compounds benefits from its oxygen- and solvent-free conditions that can avoid unwanted dissociation of the reaction products.

The recent advent of the laser vaporization method combined with molecular beam techniques has opened up a different aspect of organometallic chemistry. The laser vaporization method enables atoms, dimers, and various clusters (consisting of up to 1000 atoms) to be produced in considerably higher density in a short period [31]. When the laser vaporization products adiabatically expand into a vacuum with high-pressure carrier gas of helium (or other rare gases), they are allowed to form well-collimated, thermalized cluster beams that are ideal for studying their thermodynamic and kinetic properties [32–35]. Duncan and co-workers [36] produced the clusters of silver and aluminum ions with benzene by

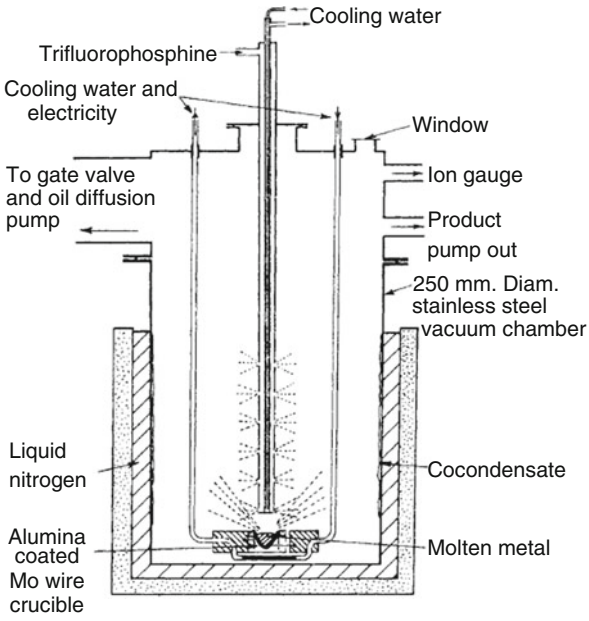

Fig. 8.3 Schematic view of a vacuum apparatus for the gas-phase synthesis of organometallic complexes presented by Timms. (Reproduced from Ref. [26] with permission from the Royal Society of Chemistry)

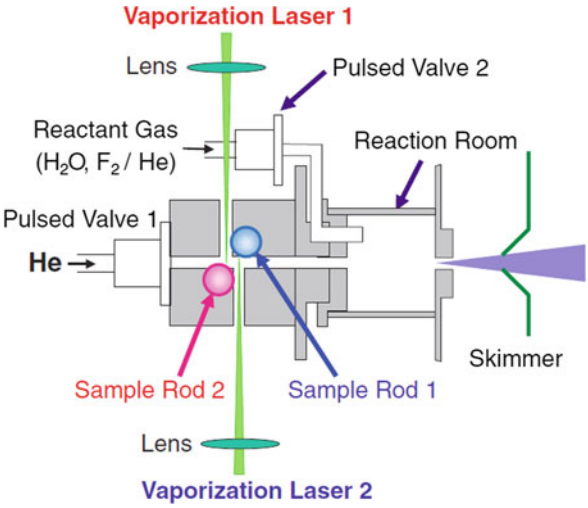

Fig. 8.4 Schematic view of a dual-laser vaporization cluster source which has two sample rods, two pulsed valves, and a reaction room. (Reproduced from Ref. [45] with permission from the Chemical Society of Japan)

means of laser vaporization and studied their photoinduced dissociation. Armentrout and co-workers [37–38] examined collision-induced dissociation of silver-benzene and first-row transition metal-benzene cluster ions. These works provided reliable thermodynamic data of the vibrational modes and dissociation energies for the clusters, which contributed to the understanding of the bonding nature between the metal atom and the benzene ligands.

In the laser vaporization method, cluster size and composition are controllable in a wide range, depending on the choice of the target material, laser fluence, carrier gas pressure, and the volume of the reaction room (sometimes called "waiting room"), where the metal vapor and the gaseous reactants are mixed in the presence of the carrier gas [39–40]. Kaya, Nakajima, and co-workers [41–42] built a dual-laser vaporization cluster source depicted in Fig. 8.4, equipped with a couple of pulsed valves, which enabled the production of clusters containing multiple elements and/or gaseous ligands. Using this cluster source, Hoshino et al. [43] synthesized polynuclear clusters of multiple vanadium atoms and benzene molecules denoted V_nBz_m and examined their structures with mass spectrometry. Interestingly, the photoionization mass spectrum in Fig. 8.5 indicated that these V-Bz neutrals were populated by magic number clusters with $m = n + 1$, each of which has one Bz molecule in excess. The chemical probe experiment showed that V_nBz_{n+1} were inert upon exposure to carbon monoxide (CO) while V_nBz_n and V_nBz_{n-1} absorbed 3 and 6 CO molecules, respectively. Since CO is regarded as a two-electron donor, three CO molecules are equivalent to one Bz ligand. Compared to V_nBz_{n+1}, it was thus thought that the addition of 3 and 6 CO molecules correspond to the lack of one and two exterior Bz molecules in the structures of V_nBz_n and V_nBz_{n-1}, respectively. These magic number behavior and reactivity suggested that V_nBz_{n+1} clusters exhibit a multiple-decker sandwich structure in which V atoms and Bz molecules are piled up alternately (see Fig. 8.5), while V_nBz_n and V_nBz_{n-1} were deduced

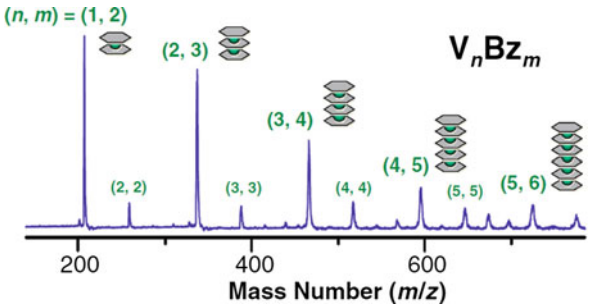

Fig. 8.5 Photoionization mass spectrum for V_nBz_m clusters. Each V_nBz_m is expressed as (n, m). The predominant peaks have magic numbered compositions of $(n, n + 1)$, and most of the minor peaks are assigned to the (n, m) clusters. Proposed structures for $(n, n + 1)$ clusters are also shown. (Reproduced from Ref. [45] with permission from the Chemical Society of Japan)

to be one- and two-end open sandwich clusters, respectively. The multiple-decker structures of cationic clusters of $V_nBz_{n+1}^+$ have later been confirmed by Bowers and co-workers with ion mobility measurements [44].

8.2.3 *Mass Spectroscopic Characterization of Transition Metal-Benzene Sandwich Clusters*

To gain detailed insights into the bonding scheme of V_nBz_{n+1} clusters, it is a good idea to address a question of how such multiple-decker sandwich formation is dependent on metal elements and ligands. To answer this question, Kurikawa et al. [46–48] synthesized a series of metal-benzene clusters, M_nBz_m, from first-row transition metals M (= Sc to Cu), and the cluster formation of these clusters was studied in the same manner as was employed for V_nBz_m clusters. For Co_nBz_m clusters, photoionization mass spectroscopy revealed that, in the series of the abundant clusters, the number of Co atoms increased one by one, whereas the number of Bz molecules did not necessarily increase with the cluster size (Fig. 8.6g). Namely, every n had a specific maximum number of Bz molecules adsorbed (m_{max}). The magic number clusters such as $(n, m) = (1, 2)$, $(2, 3)$, $(3, 3)$, $(4, 4)$, $(5, 4)$, and $(6, 4)$ did not react with ammonia molecules. However, most of these clusters cannot be expressed as $(n, n + 1)$ and thus are unlikely to take a sandwich structure. It was deduced that they exhibit a so-called "rice-ball" structure, where the Co_n core is surrounded by the Bz molecules, as depicted in Fig. 8.7b [46–47]. A similar mass spectral trend (in m_{max}) was seen for the Bz complexes of other late transition metals of Fe and Ni, while Sc_nBz_m and Ti_nBz_m were distributed over the $(n, n + 1)$ composition (see Fig. 8.6). Thus, the following two types of structures are concerned with transition metals M: the multiple-decker sandwich structure is characteristic of the complexes for early transition metals (M = Sc to V), whereas

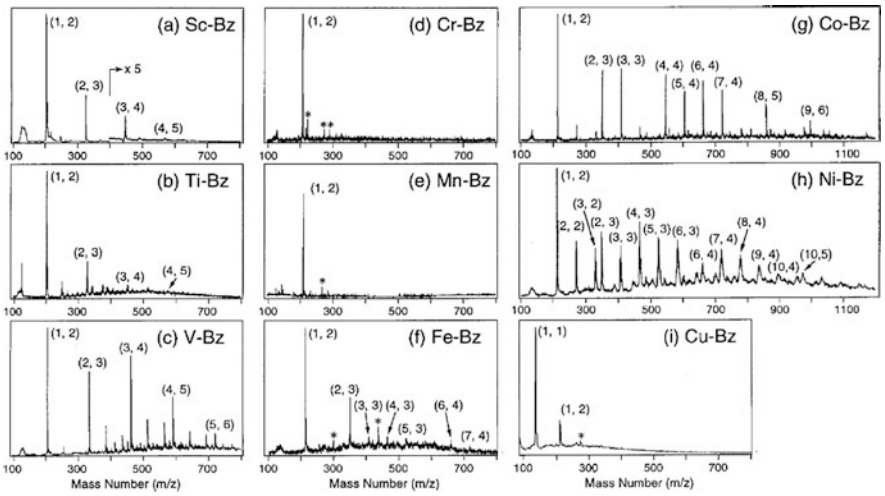

Fig. 8.6 Photoionization mass spectra for M_nBz_m clusters (M = 3*d* transition metals: (**a**) Sc, (**b**) Ti, (**c**) V, (**d**) Cr, (**e**) Mn, (**f**) Fe, (**g**) Co, (**h**) Ni, and (**i**) Cu). Each M_nBz_m is expressed as (*n*, *m*). The asterisks denote the contamination peak of oxide. (Reprinted with permission from Ref. [48]. Copyright 1999 American Chemical Society)

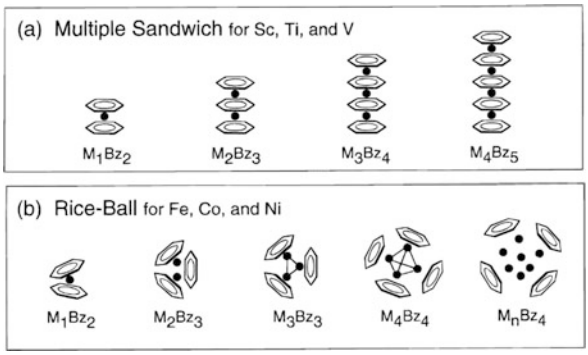

Fig. 8.7 (**a**) Proposed structures for early transition metals for Sc, Ti, and V; multiple sandwich. (**b**) Proposed structures for late transition metals from Fe to Ni; rice-ball. (Reprinted with permission from Ref. [48]. Copyright 1999 American Chemical Society)

the rice-ball structure is formed for late transition metals (M = Fe to Ni). Cr, Mn, and Cu belong to neither of the two metal groups: they did not produce any larger clusters than mononuclear MBz_2 in the reaction with Bz (see Fig. 8.6d, e, i) [48].

To probe basic concepts underlying the metal-ligand interactions, transition metal-fullerene (C_{60}) cluster ions, $M_n(C_{60})_m^+$ (M = Sc, Ti, V, Cr, Mn, Fe, Co, and Ni), were prepared by means of laser vaporization and studied with mass spectrometry [11, 49–53]. Among the transition metals studied, Nakajima et al. [51, 53] found that $M_n(C_{60})_m^+$ with M = Sc, Ti, and V were populated by (*n*, $n + 1$) and (*n*, *n*) clusters, which did not form a carbonyl complex. It was proposed that the structures of the predominant clusters are chain-like multiple dumbbell or ring structures (Fig. 8.8), analogous to multiple-decker sandwich clusters. In

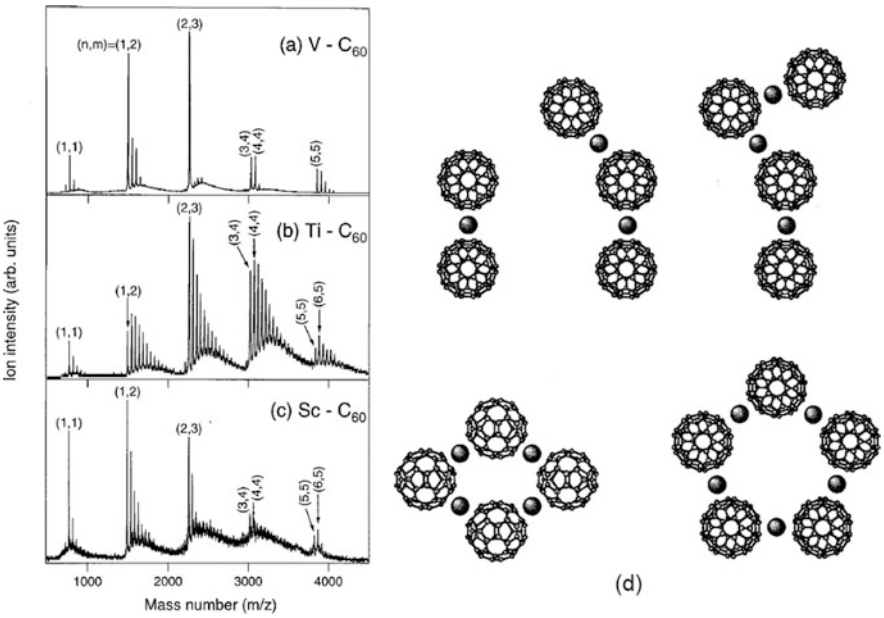

Fig. 8.8 Left: typical photoionization mass spectra of (**a**) $V_n(C_{60})_m$, (**b**) $Ti_n(C_{60})_m$ and (**c**) $Sc_n(C_{60})_m$. Right: (**d**) proposed dumbbell and ring structures for $M_n(C_{60})_m$ (M = Sc, Ti and V). (Reprinted with permission from Ref. [11]. Copyright 2000 American Chemical Society)

contrast, $M_n(C_{60})_m^+$ with the other metals exhibited a different mass feature. Nagao et al. [52] proposed that $Co_4(C_{60})_4^+$ exhibit a face-centered tetrahedron structure (Fig. 8.9) that is again analogous to the rice-ball structure of Co_4Bz_4. Such face-centered structures are thought to be prevalent in $M_n(C_{60})_m^+$ where M = Cr, Fe, Co, and Ni [11, 53]. Metal-coronene ($C_{24}H_{12}$) clusters, $M_n(C_{24}H_{12})_m$, have also attracted much interest, as their ions consisting of various metals were investigated. Pozniak and Dunbar [54] studied the reactivity of more than 20 metal ions toward coronene and classified these ions into 2 groups depending on whether the reaction led to the (1, 2) formation. Many of the transition metals such as Sc^+, Ti^+, Cr^+, Mn^+, Fe^+, Ni^+, and Cu^+ allowed yielding $M(C_{24}H_{12})_2^+$ that was deduced to be a sandwich complex. Duncan and co-workers [55–57] conducted photodissociation measurements on $Fe_n(C_{24}H_{12})_m^+$ and $Cr_n(C_{24}H_{12})_m^+$ and evidenced possible sandwich structures for these cluster ions, including the multiple-decker $Cr_2(C_{24}H_{12})_3^+$ cluster. $V(C_{24}H_{12})_2^-$ and $Ti(C_{24}H_{12})_2^-$ anions were also assigned to be sandwiches [58]. Nakajima, Kaya, and co-workers studied vanadium complexes with substituted benzene, $V_n(\text{arene})_m$ (arene = toluene, $C_6H_5CH_3$, and fluorobenzene, C_6H_5F) [59] and their mononuclear anions $V(\text{arene})_m^-$ ($m = 1, 2$) [60], as well as $Sc(C_6H_5CH_3)_m^-$ ($m = 1, 2$) [61], and demonstrated that the arene's electron-donating or electron-withdrawing property shifts the energy levels of its valence orbitals that affect the production efficiency of these clusters. Although

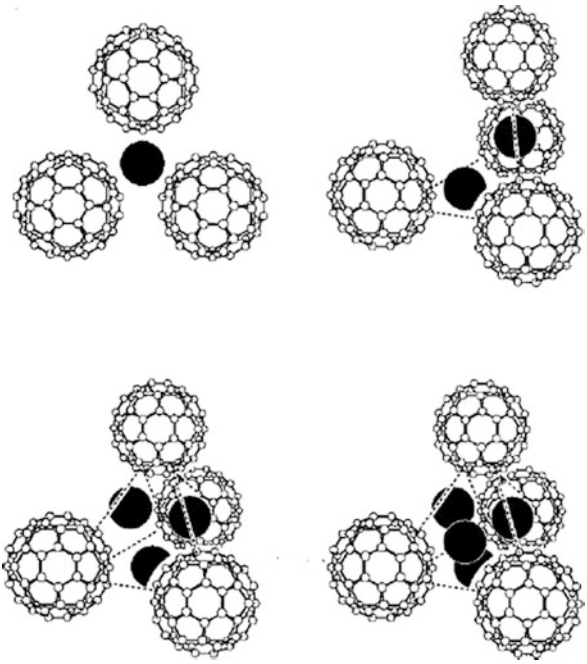

Fig. 8.9 Proposed face-centered structures for $M_n(C_{60})_m$ (M = Cr, Fe, Co, and Ni). (Reprinted with permission from Ref. [11]. Copyright 2000 American Chemical Society)

electrostatic interactions might partly contribute to the bonding of the ion-molecule complexes, these studies reinforced that the orbital interactions between the metal *d* and Bz π electrons are responsible for the M-Bz bonding in the M_nBz_m clusters.

It is then postulated that the stability of the M-Bz sandwich formation is balanced by the antibonding character resulting from the orbital interactions. The simplest examples are mononuclear MBz_2 clusters, the structures of which are described with the 18-electron rule in the same manner as those of metallocenes. While $CrBz_2$ satisfies the 18-electron rule by filling its bonding (e_{2g}) and nonbonding (a_{1g}) orbitals, MBz_2 clusters with the late transition metals of M = Mn to Ni violate the rule due to the excess 3*d* electrons that should occupy the antibonding orbitals with e^*_{1g} symmetry. It is known that such extra electrons in the e^*_{1g} orbitals induce a Jahn-Teller instability which may distort the sandwich structure from the highest (D_{6h} or D_{6d} in case of MBz_2) symmetry to a lower one to remove the degeneracy [20]. This effect lowers the M-Bz binding energy compared to that of a M-M bond in case of multinuclear complexes, leading to the rice-ball formation for the late transition metals rather than the multiple-decker sandwich formation. In the rice-ball structures, m_{max} is governed not only by electronic but also by geometric factors, and it is basically lower than the value expected from the total number of valence electrons, as the steric hindrance between Bz molecules becomes more crucial at large *n* [48].

In contrast, all the transition metals of M = Sc to Cr allow MBz_2 complexes which have no more than 18 valence electrons, but the production efficiency of

the multiple-decker sandwich clusters is quite metal-dependent, as depicted in Fig. 8.6. Yasuike et al. [62] demonstrated that the sandwich formation is affected not only by a thermodynamic but also by a kinetic factor, where the formation process governs the reactivity rather than the thermodynamic stability of the reaction products does. In particular, the spin multiplicity of the system has been proven to be an important guideline in understanding the reactivity of transition metal ions [63]. They carried out quantum chemical calculations to determine the most preferable spin states for reactant and product clusters in the cluster growth process of $M_nBz_{n+1} + M \rightarrow M_{n+1}Bz_{n+1}$ ($n = 1, 2$), where M = Ti, V, and Cr. According to the calculation results, both $CrBz_2$ and Cr_2Bz_2 preferred a singlet state, whereas the ground state of a Cr atom is septet [64]. This means that multiple-step nonadiabatic (i.e., spin-flip) transitions are needed for the growth from $CrBz_2$ to Cr_2Bz_2 as the overall reactant system ($CrBz_2 + Cr$) does not conserve its total spins during the reaction. By contrast, the calculation results estimated the lowest-energy state of V_2Bz_2 to be either a singlet or triplet, which is close in energy to each other. VBz_2 was determined to be a doublet while the ground state of a V atom is a quartet [64]. Therefore, spin flipping is not required for the transition from $VBz_2 + V$ to the triplet-state V_2Bz_2. The reaction barrier arising from the spin conservation rule explains the absence of Cr_2Bz_2 and larger clusters, while the efficient production of V_nBz_{n+1} is likely due to spin conservation in the cluster growth process.

8.3 Electronic and Magnetic Properties of Transition Metal-Benzene Sandwich Clusters

8.3.1 Physical Properties of Low-Dimensional Materials

It has been known that properties of materials which have low-dimensional (i.e., zero-, one-, and two-dimensional, hereafter 0D, 1D, and 2D, respectively) structures are different from those of three-dimensional (3D) materials such as bulk materials [65]. For instance, fullerenes, carbon nanotubes, and graphene (Fig. 8.10) are regarded as typical low-dimensional materials that are distinguished from graphite. There has been tremendous interest in extraordinary electron motion and resulting unique electronic properties originating from the low dimensionality of these materials. In fact, conductivity of carbon nanotubes has been a stimulating subject, since it was shown that nanotubes with a certain chirality (i.e., degree of twist) exhibit dramatically high conductivity [66–67]. It is understood that electron transport in the nanotubes is an anisotropic phenomenon in which different periodic boundary conditions are applied depending on the chirality [68]. Likewise, low-dimensional magnetism has gathered continuous attention since the discovery of the first single-molecule magnet (SMM), which exhibited magnetic hysteresis of a pure molecular origin [69]. Mn-containing SMMs have been studied for decades because the high-spin ($3d^5 4s^2$) configuration of a Mn atom is advantageous

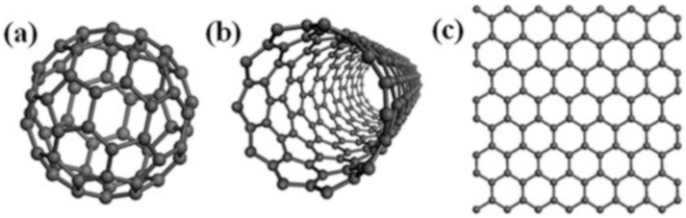

Fig. 8.10 Typical structures of (**a**) fullerene, (**b**) carbon nanotube, and (**c**) graphene as representatives for 0D, 1D, and 2D materials, respectively. (Reproduced from Ref. [79] with permission from the Royal Society of Chemistry)

for maximizing the spin multiplicity of SMMs. However, it is noted that better performing SMMs, with a large energy barrier to magnetic relaxation, require not only a high-spin ground state but also a large magnetic anisotropy. Such SMMs have often been achieved by strategic choices of bridging ligands that induce effective exchange interactions with a large anisotropy in the metal-ligand system [70–73]. Recently, 1D polymer chains called single-chain magnets (SCMs) have been demonstrated to show magnetic properties analogous to those of 0D SMMs [74–75]. These electronic and magnetic properties of low-dimensional materials have also motivated lots of studies aimed at their technological applications for molecule-based semiconductors [76], spintronics devices [77–78], energy storage media [76], high-density information storage devices [77], and so on.

8.3.2 Low Dimensionality of Transition Metal-Benzene Sandwich Clusters

The design of functional nanomaterials benefits more and more from a bottom-up approach that utilizes clusters as building blocks. Dimensionality plays an important role in defining the properties of nanomaterials. The controlled assembly of clusters facilitates the fabrication of materials with tailored dimensionality, that is, with tailored functionality [45, 80–81]. In order to explore, identify, and tune the functionality via the bottom-up approach, on the other hand, it is essential to understand the intrinsic properties of clusters themselves.

At this point, transition metal-Bz sandwich clusters can be ideal building blocks for low-dimensional functional nanomaterials. For instance, mononuclear MBz and MBz_2 clusters are regarded as motifs for organic surface-supported metal atoms, the magnetic moments of which have been of great interest [82]. Pandey et al. [83–84] calculated magnetic moments for MBz and MBz_2 complexes (M = Sc-Ni) and showed that the first and second Bz molecules differently interact with the electrons of the M atom. According to the calculation result, some MBz complexes (M = Sc, Ti, and V) have a high magnetic moment. The second Bz addition quenches the

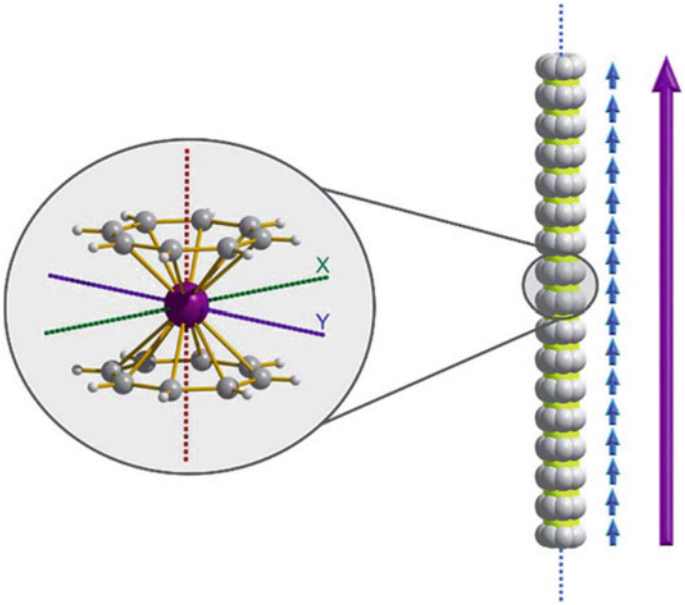

Fig. 8.11 A hypothesized chain-like arrangement of $M(COT)_2$ monomers with uniaxial magnetic anisotropy, illustrating the concept of modular design of SCMs. The axial anisotropy of each monomer is depicted as blue vectors, and the vector addition of the monomeric axial anisotropies yields the net axial anisotropy (purple). (Reproduced from Ref. [86] with permission from the Royal Society of Chemistry)

electron spins of MBz, and one unpaired electron remains in the odd-electron systems of $ScBz_2$ and VBz_2. Indeed, the electron paramagnetic resonance (EPR) measurement by Elschenbroich et al. [85] confirmed that VBz_2 derivatives which have an interannular bridge are paramagnetic with a spin multiplicity of $2S + 1 = 2$. Moreover, multiple-decker sandwich clusters can be viewed as single atomic chains, where an important question should be addressed how the electron spins of each metal atom interact with those of each other. It is hypothesized that a modular design of SCMs may be feasible if each $M(COT)_2$ monomer with uniaxial magnetic anisotropy is aligned along with the primary (z) axis (Fig. 8.11) [86]. The Stern-Gerlach experiment [87] carried out by Miyajima et al. [88–90] provided direct insights into magnetic properties of multiple-decker sandwich clusters. Importantly, the experiment reported that the magnetic moments of V_nBz_{n+1} monotonically increased with increasing cluster size (Fig. 8.12). In contrast, the magnetic moments of Co_nBz_m clusters, measured in the same manner, showed a quenching effect with increasing n and m [91]. This difference somewhat illustrates that the multiple-decker formation can stabilize the ferromagnetic ordering of the electron spins contained on metal atoms.

Recent advances in theoretical chemistry and computer resources have allowed computations of geometric and electronic structures of even large, multinuclear

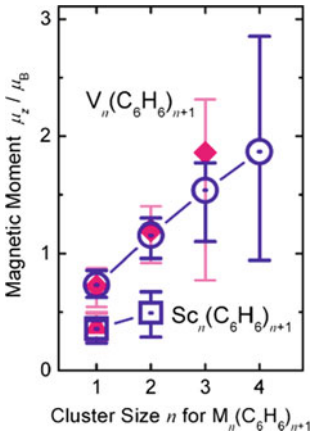

Fig. 8.12 Magnetic moments μ_z for V_nBz_{n+1} clusters measured by the Stern-Gerlach experiment. Those for Sc_nBz_{n+1} are also plotted. Open circles/squares indicate the magnetic moments determined at ~150 K, whereas filled diamonds indicate the magnetic moments at room temperature. (Reprinted with permission from Ref. [90]. Copyright 2007 American Chemical Society)

transition metal-Bz clusters. Kandalam et al. [92] employed density functional theory (DFT) to optimize the structures for V_nBz_{n+1} clusters up to $n = 3$. Upon comparison of the total energies between the sandwich and rice-ball V_2Bz_3 clusters, they confirmed that the sandwich formation was lower in energy than the rice-ball cluster at any possible spin multiplicity. In addition, the simulated spin multiplicities of V_nBz_{n+1} ($n = 1$–3) exhibited a linear increase, in agreement with the experiment described above. Shortly after this work, Wang et al. [93] extended calculations up to V_5Bz_6 and confirmed the size evolution of magnetic moment in this size range. They also reported that, regardless of cluster size and the position of the atom, each V atom possesses a magnetic moment of slightly larger than 1 Bohr magneton (μ_B). In contrast, each Bz molecule has a small negative magnetic moment. This counterbalancing illustrates that not only VBz_2 but also each VBz unit has a magnetic moment of 1 μ_B, resulting in the size-dependent increase of the total magnetic moment. On the other hand, rice-ball Co_nBz_m clusters such as $(n, m) = (3, 3)$ and (4, 4) have been calculated to have antiferromagnetic nature [94], which does not contradict their small magnetic moments determined in the experiment [91]. Furthermore, various infinite sandwich wires composed of metal atoms and arene molecules have been theoretically investigated [95–105]. Particularly, early works simulated the density of states in the V-Bz wire and proposed that the V-Bz wire is a half-metallic ferromagnet [95–99], where only one spin channel is metallic owing to the insulating band gap in the opposite spin channel (see Fig. 8.13). Such half metallicity of the sandwich wires has made metal-organic sandwich complexes promising candidates for organic spintronics, where the spin-polarized signal can be mediated and controlled by organic molecules in a 1D wire form. It should be noted that, in terms of their electronic and magnetic properties, organic half metals are especially useful for organic spintronics, because 100% spin polarization transportation is then available.

Despite the successes of these computational studies, it should be emphasized that, for many theories including the widely used DFT, there is still room for

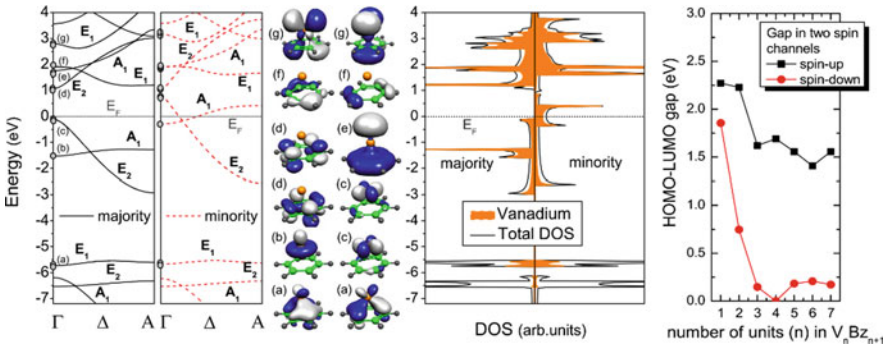

Fig. 8.13 The calculated spin-resolved band structure (left plot) and the DOS (plot in the middle) of the V-Bz wire in the ferromagnetic phase. The labels at the band structure refer to crystalline orbitals of the wire calculated for the Γ point, which are depicted on the right of the plot. The right panel shows values of the HOMO-LUMO gap in two spin channels for V_nBz_{n+1} as a function of n. (Reproduced from Ref. [97] with permission from the American Physical Society)

improvement in the reliability of magnetic moments and other spin-dependent properties [106–108]. In fact, the DFT methods for even small organometallic systems have the specific problem that the spin multiplicity of a global minimum structure depends on the employed functional. Recently, the quantum Monte Carlo (QMC) method has offered accurate calculations for spin-dependent properties of VBz [106] and V_nBz_{n+1} ($n = 1$–3) [109] systems. Such higher-level theories, however, are much computationally demanding and are not universally applicable when compared to the DFT. Here, combining computational methods with experiments is an effective approach. Quantum chemical calculations provide various kinds of simulated action spectra that are structure- and electronic state-dependent. Through the comparison between simulated and experimental spectra, the correctness of the calculations can be verified within a reasonable level of theory. In this way, the calculation results, which show the same fingerprints as the experiments do, give information on plausible structures and electronic and magnetic properties.

For the electronic and magnetic characterization of transition metal-Bz sandwich clusters, notable progress has indeed been made by joint experimental and theoretical studies. The details and outcomes of these studies are described in the following subsections.

8.3.3 *Laser Spectroscopic Studies of Transition Metal-Benzene Sandwich Clusters*

Among physical quantities that give direct insights into the valence electronic structure of a molecule, ionization energy (IE) and electron affinity (EA) are of particular importance. IE reflects the energy level of the highest occupied

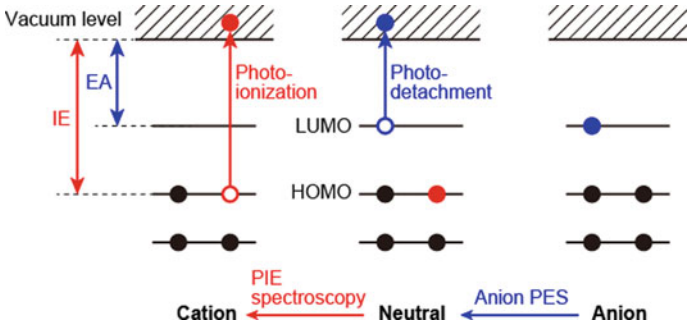

Fig. 8.14 Schemes of photoionization efficiency (PIE) spectroscopy and anion photoelectron spectroscopy (PES). Filled circles represent electrons that occupy valence orbitals. The HOMO and LUMO stand for those of the neutral state. For simplicity, the neutral is a singlet state with a closed-shell configuration, and it is assumed that there is no significant relaxation of the electronic structure during the electronic transitions

molecular orbital (HOMO), whereas EA is related to the energy level of the lowest unoccupied molecular orbital (LUMO). Experimental IE and EA values for a cluster are accessible by gas-phase laser spectroscopies. Photoionization efficiency (PIE) spectroscopy measures PIE as a function of photon energy. The PIE curve exhibits an onset whose energy gives the IE value for the neutral. Anion photoelectron spectroscopy (PES) estimates the binding energy of the excess electron of an anion by measuring the kinetic energy of the photoelectron (photodetached electron, PE). Within the limits of Koopmans' theorem, the observed photoelectron originates from the LUMO of the neutrals, which is occupied for the corresponding anions, so the EA of the neutral is obtained in this way. The energetic relationship between IE and EA is depicted in Fig. 8.14, along with the schemes of PIE spectroscopy and anion PES.

The PIE curves have been measured for V_nBz_{n+1} sandwich clusters with up to $n = 5$, showing that the IE monotonically decreased with increasing cluster size, as depicted in Fig. 8.15 [43, 110]. For larger clusters with $n \geq 4$, the PIE measurements also determined second lowest IEs that reflect the ionization from the next HOMO (HOMO – 1). The second lowest IEs exhibited a similar decrease seen for the lowest IEs [110]. Yasuike and Yabushita [111] employed the extended Hückel molecular orbital method to compute electronic structures of V_nBz_{n+1} clusters. Like those of ferrocene, the valence orbitals computed for V_nBz_{n+1} are classified into three types in terms of symmetry matching. dδ orbitals, which are combinations of the $3d_{xy}$ or $3d_{x^2-y^2}$ orbitals of V atoms and their symmetry-matching π orbitals of Bz molecules, form a quasi-band electronic structure as shown in Fig. 8.16, resulting in a monotonic decrease in IE with an increasing number of n. Importantly, the calculated IEs for V_nBz_{n+1} agreed well with the experimental values from the PIE spectra, thus reinforcing the theory employed in the calculations. In a general sense, such IE decrease has been known as a common phenomenon in multiple-decker

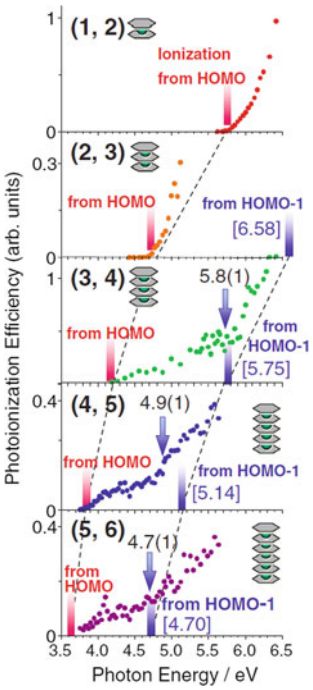

Fig. 8.15 Photoionization efficiency (PIE) spectra of V_nBz_m for $(n, m) = (1, 2)$ to (5, 6). The first onset corresponds to the ionization energy (IE) for removing an electron from the HOMO. As well as the first onset, a second ionization onset was observed as the change of slope in the PIE curves of (3, 4), (4, 5), and (5, 6) to be 5.8 ± 0.1, 4.9 ± 0.1, and 4.7 ± 0.1 eV, respectively. The second onsets represent second lowest IE that can be explained by ionization processes from the next HOMO (HOMO – 1). The onsets predicted by the quasi-band electronic structure are also shown in brackets. (Reproduced from Ref. [45] with permission from the Chemical Society of Japan)

structures of M_nBz_{n+1} (M = Sc, Ti, and V) [48], as it was not observed for other species such as Co_nBz_m that prefers a rice-ball structure at large n [46–48].

On the other hand, Judai et al. [60–61] conducted their pioneering works by applying anion PES to transition metal-arene complex anions. A magnetic bottle-type PE spectrometer was used in their experimental setup (shown in Fig. 8.17), as PEs can be collected at high efficiency in this method. Their PE spectra for mononuclear VBz^- and derivatives, $V(arene)^-$ (arene = toluene, $C_6H_5CH_3$, and fluorobenzene, C_6H_5F), taken with 355 nm (3.49 eV) laser radiation, are shown in Fig. 8.18. In the figure, the horizontal axis corresponds to electron binding energy (EBE), which is defined as EBE = $h\nu$ – EKE, where $h\nu$ is a photon energy of the detachment laser and EKE is an electron kinetic energy. Each arrow indicates the threshold binding energy, which corresponds to the upper limit of EA. The binding energy at each peak center represents a vertical detachment

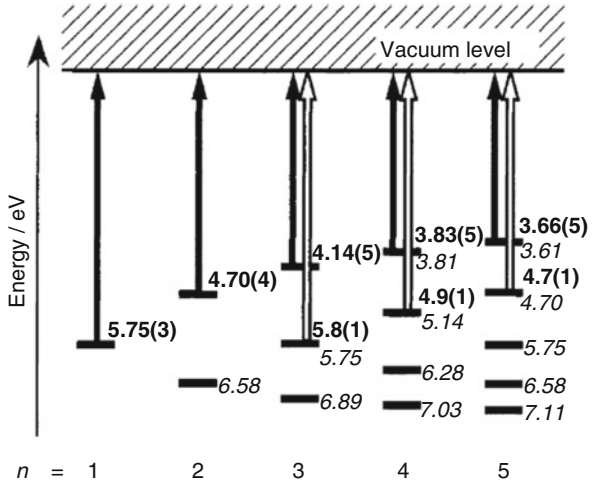

Fig. 8.16 Quasi-band electronic structure of valence orbitals of V_nBz_{n+1}. Bold-faced numbers indicate experimental values in eV with uncertainties in parentheses; 5.75(3) represents 5.75 ± 0.03 eV. Calculated values obtained by the simple Hückel model are given in italics. Solid and open arrows indicate the lowest and the second lowest ionization processes from each HOMO and HOMO – 1, respectively. They also correspond to the ionization processes observed in the PIE spectra of Fig. 8.15, respectively. (Reprinted with permission from Ref. [110]. Copyright 2002 American Chemical Society)

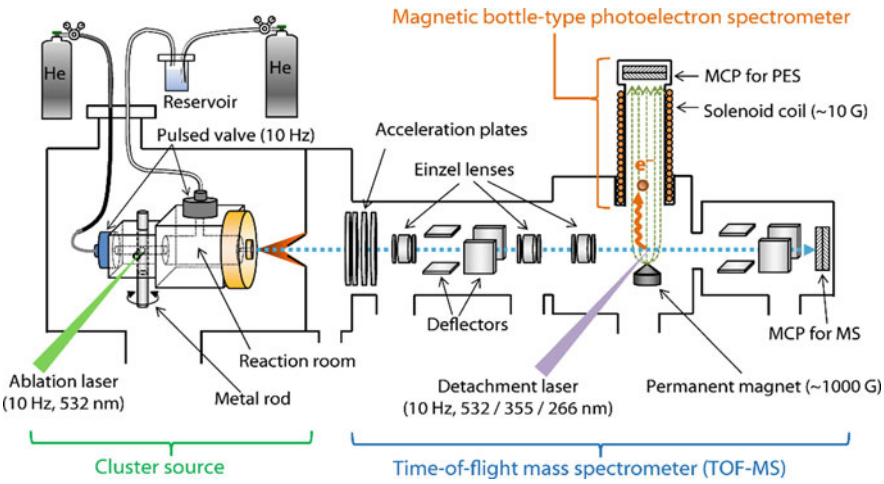

Fig. 8.17 An experimental setup for anion PES equipped with a time-of-flight mass spectrometer for metal-organic cluster anions. Lasers, valves, and high-voltage electronic pulses are controlled by a digital delay generator

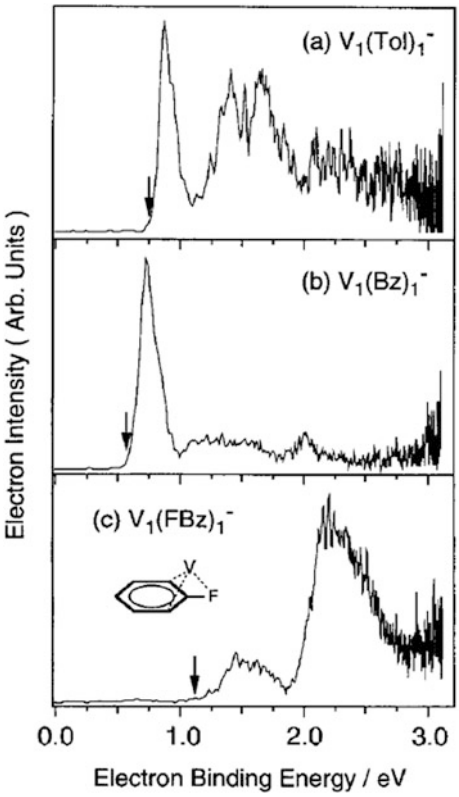

Fig. 8.18 Anion PE spectra of (**a**) $V(C_6H_5CH_3)^-$, (**b**) VBz^-, and (**c**) $V(C_6H_5F)^-$ taken with 355 nm (3.49 eV) radiation. Vertical arrows indicate onset energies. In (**c**), the presumed structure for $V(C_6H_5F)^-$ is shown. (Reprinted from Ref. [60] with permission from Elsevier)

energy (VDE), at which the geometry of the cluster anion is unchanged during the photodetachment process. The broadness of the peak reflects the Franck-Condon overlap between the vibrational ground state of the anion and that of the corresponding neutral. For example, the sharp and intense peaks in Fig. 8.18a, b show that $V(C_6H_5CH_3)^-$ and VBz^-, respectively, do not significantly change their structures upon photodetachment. This spectral feature is often ascribed to possible photodetachment from a nonbonding orbital electron at the anionic state. Indeed, the molecular orbital diagram of VBz^- showed that the HOMO of the anion is a nonbonding orbital with a_1 symmetry [60]. By contrast, $V(C_6H_5F)^-$ exhibited a broad feature in its PE spectrum (Fig. 8.18c). It is thus conceivable that its structure (see the inset of Fig. 8.18c) may be somewhat different from the half-sandwich structures of VBz^- and $V(C_6H_5CH_3)^-$. Another interesting feature is the lack of VBz_2^- in the mass spectrum. The molecular orbital theory showed that both of the HOMO and LUMO of VBz_2 are nonbonding orbitals. The absence of VBz_2^- is thus ascribed to the negative EA of VBz_2, meaning that the excess electron does not lower the energy of VBz_2^-.

8.3.4 *Joint Anion Photoelectron and Computational Studies of Vanadium-Benzene Sandwich Clusters and Their Anions*

The interplay between anion PES and theory, as described in Sect. 8.3.3, is especially powerful to study clusters both at anionic and neutral states. However, applications of this method for transition metal-Bz sandwich clusters were somewhat limited due to difficulty in preparing anions of the transition metal-Bz clusters. Despite their successful work on VBz^-, Judai et al. did not investigate multinuclear $V_nBz_m^-$ anions. Their mass spectrum (Fig. 8.19a) showed some dehydrogenation products with no presence of $V_nBz_m^-$ with $n \geq 2$ and $m \geq 2$.

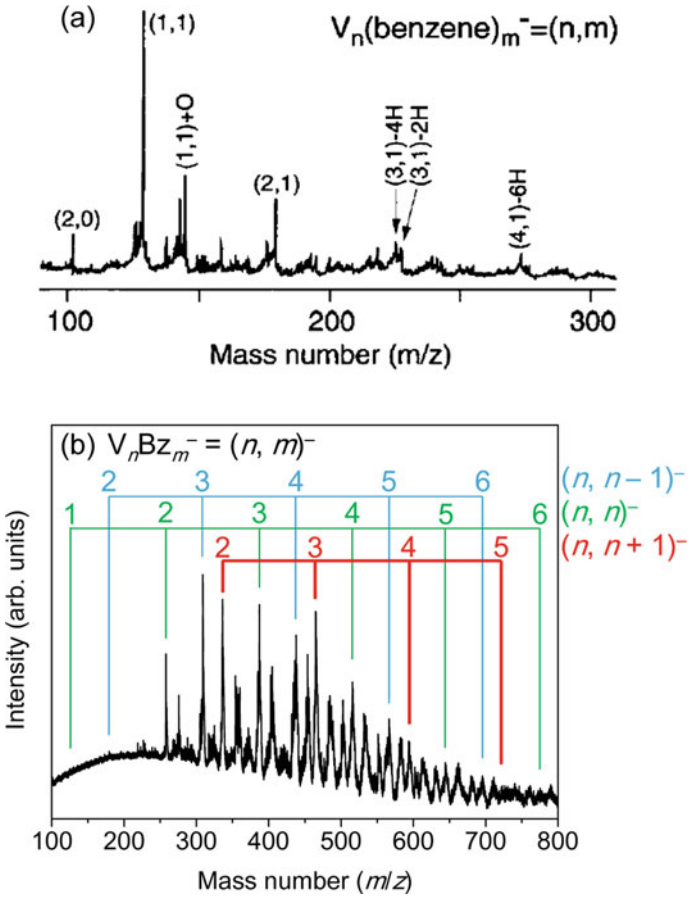

Fig. 8.19 Mass spectra of $V_nBz_m^-$ cluster anions measured by (**a**) Judai et al. [60] and (**b**) Masubuchi et al. [113] The maximum stagnation pressures of He carrier gas used for cluster production were 10 bar and 50 bar for (**a**) and (**b**), respectively. (**a**) was reprinted from Ref. [60] with permission from Elsevier and (**b**) from Ref. [113] with the permission of AIP Publishing

The dehydrogenation channels may be characteristic of transition metal-Bz cluster ions as they have also been found in the reaction of V_n^+ with deuterated benzene (C_6D_6), where deuterium-poor clusters $V_nC_6D_k^+$ ($k = 0, 2, 4$) were detected [112]. Nevertheless, we recently succeeded in the gas-phase synthesis of $V_nBz_m^-$ anions without dehydrogenated species [113]. In the mass spectrum of Fig. 8.19b, the peaks of $V_nBz_m^-$ are denoted by the notation $(n, m)^-$, and the number above each peak indicates the number of V atoms, n. $V_nBz_{n+1}^-$ ($n \geq 2$) and some other kinds of anions such as $V_nBz_{n-1}^-$ ($n \geq 2$) and $V_nBz_n^-$ ($n \geq 1$) are the most abundant, though the other peaks are assigned to $V_nBz_m^-$ combined with oxygen or water molecules. We adopted a high-pressure Even-Lavie pulsed valve [114] to load He carrier gas at a stagnation pressure of 50 bar, which is approximately five times higher than that in the former experiments (~10 bar at maximum). The Even-Lavie valve is known to generate cold molecules whose rotational temperature is even lower than 1 K [114]. It is thus reasonable that such high pressure promotes further cooling down of $V_nBz_m^-$ anions to avoid unwanted dehydrogenation.

The joint anion PE and computational method was first employed for Bz-rich the anionic series of $V_nBz_{n+1}^-$ ($n \geq 2$), henceforth $(n, n+1)^-$ [113]. The question in this study was whether $V_nBz_{n+1}^-$ anions exhibit multiple-decker structures with high-spin characteristics in common with the corresponding neutrals. The PE spectra for $(n, n+1)^-$ ($n = 2$–5), taken with various photon energies, are shown in Fig. 8.20. The 532 nm spectra in Fig. 8.20a–d, having a better resolution at a particular EBE than that with larger photon energy, exhibit a monotonic increase of EA with increasing cluster size, as indicated by the vertical arrows. On the other hand, the EAs of $(n, n+1)$ ($n = 1$–5) were calculated by means of the DFT, where all the possible spin multiplicities of the neutrals and anions were assessed. The EA of VBz_2 was calculated to be negative, in agreement with the work by Judai et al. [60] Moreover, the calculated EAs at $n = 2$–5, marked by the vertical lines in Fig. 8.20a–d, showed the best matches with the experimental EAs when the lowest-energy $V_nBz_{n+1}^-$ anions were featured by monotonically increasing spin multiplicities denoted as $2S + 1 = n$.

The DFT calculations also give optimized geometries, molecular orbital energy levels, and HOMO and LUMO pictures of the neutrals and anions, as displayed in Fig. 8.21a, b, respectively. For the neutrals, both the HOMOs and LUMOs belong to the minority spin. At $n = 1$–3, the HOMOs are degenerate dδ orbitals, while the LUMOs are nonbonding dσ orbitals that are mostly composed of the $3d_z^2$ orbitals of the V atoms. At $n = 4$ and 5, on the other hand, the Jahn-Teller effect lowers the D_{6h} symmetry of the multiple-decker structure, as described previously by Wang et al. [93] This also removes the degeneracy of the dδ orbitals. Because of their close energies, the dδ and dσ orbitals are hybridized, making the orbital pictures a bit complicated. However, this minor effect does not change the persistent multiple-decker formation with the ferromagnetic spin ordering even at larger n. For the anions, the comparison between Fig. 8.21a, b reveals that, except mononuclear singlet $(1, 2)^-$, the $(n, n+1)^-$ anions have ferromagnetic multiple-decker sandwich structures similarly to the corresponding $(n, n+1)$ neutrals. The excess electron occupies a dσ orbital for $n = 1$–3, a hybridized orbital consisting of dδ and dσ for

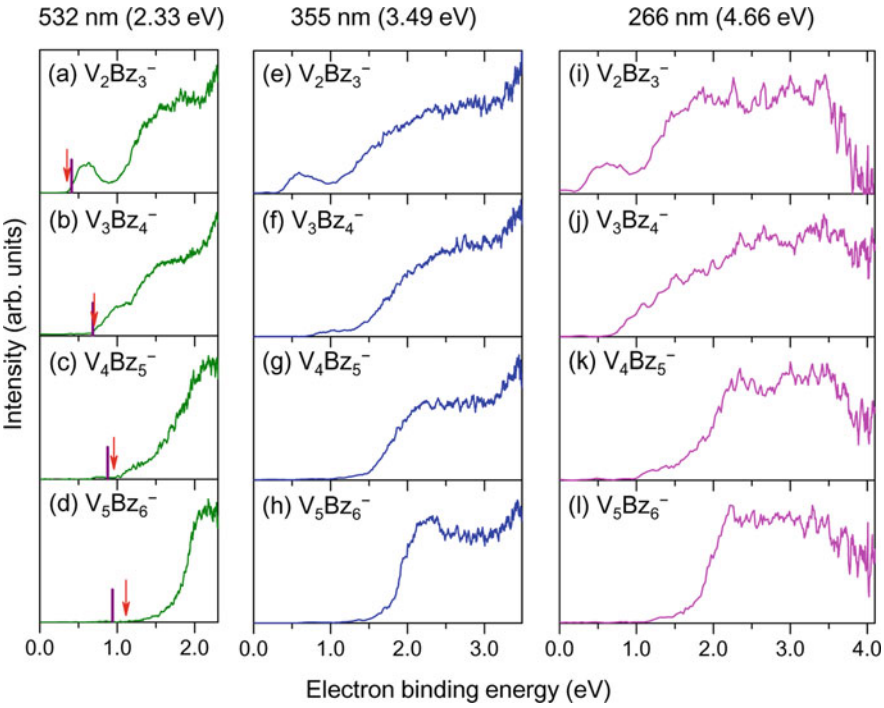

Fig. 8.20 Anion PE spectra of $V_nBz_{n+1}^-$ ($n = 2$–5) clusters taken with (**a**–**d**) 532 nm (2.33 eV), (**e**–**h**) 355 nm (3.49 eV), and (**i**–**l**) 266 nm (4.66 eV) radiation. Vertical arrows indicate the onsets of the spectra corresponding to the 532 nm spectra, while vertical lines indicate the calculated adiabatic EA values of the neutral species. (Reprinted from Ref. [113], with the permission of AIP Publishing)

$n = 4$, and again a dσ orbital for $n = 5$, all of which are delocalized along with the V atoms one-dimensionally. Importantly, for both the neutrals and anions, both the HOMOs and LUMOs belong to the minority spin, and the HOMO-LUMO gap with the majority spin is much larger than that with the minority spin irrespective of n, as plotted in the insets of Fig. 8.21. Our results not only are consistent with the former studies which have theoretically discussed the neutral V_nBz_{n+1} system [93, 97–98] but also include new experimental insights into the anionic system that can be produced during electron transport. Taken together, it can be expected that, when carrying current through a V_nBz_{n+1} cluster coupled to two electrodes, only one direction of spin will be transportable in the V_nBz_{n+1} system, hopefully leading to future spintronic applications of these sandwich clusters.

The unique electronic characteristics of $(n, n+1)^{0/-}$ (neutral and anion) clusters, as described above, originate from their one-dimensional structures. Thus, it would be interesting to determine whether eliminating Bz would change the multiple-decker sandwich structures and, more importantly, the electronic properties of such clusters. Therefore, we also acquired anion PE spectra of $V_nBz_n^-$ ($n = 1$–5),

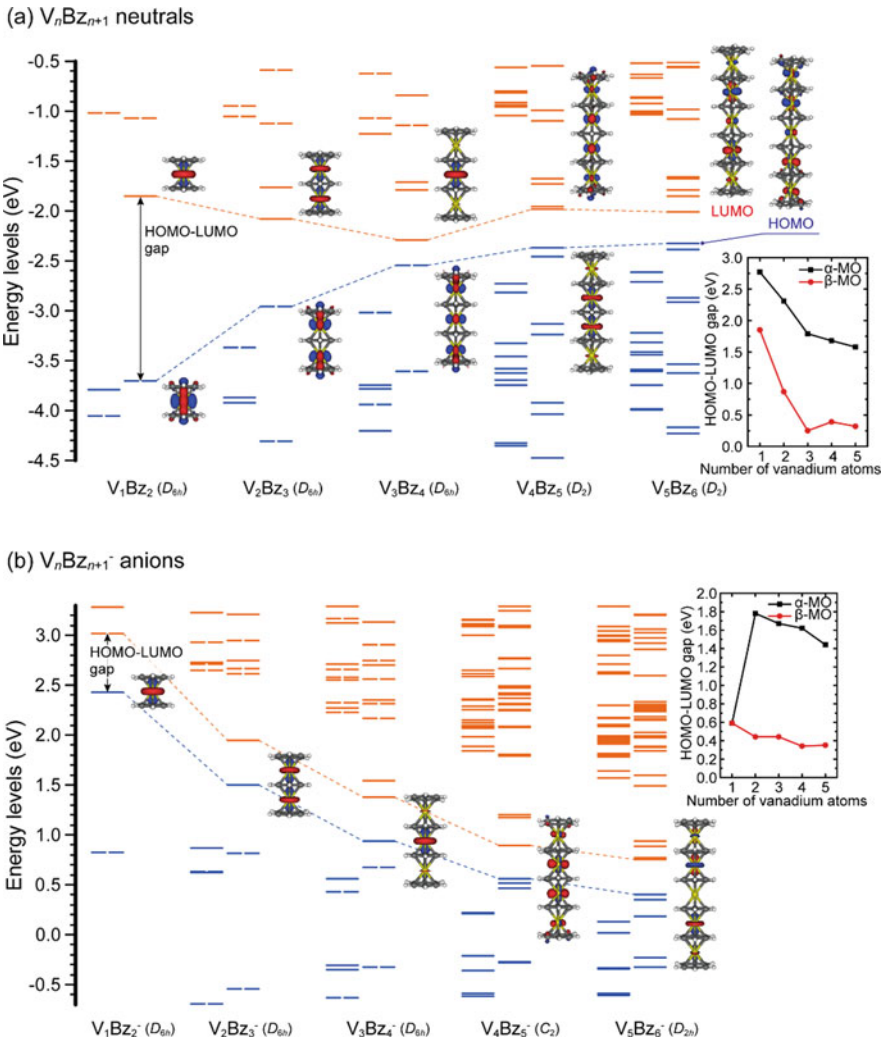

Fig. 8.21 The molecular orbital energy levels and the HOMOs and LUMOs of the lowest-energy geometries of (**a**) V_nBz_{n+1} neutrals and (**b**) $V_nBz_{n+1}^-$ anions ($n = 1$–5). The α (majority spin)-MO (left) and β (minority spin)-MO (right) are separately depicted for each cluster. The values of the HOMO-LUMO gaps in the two spin directions as a function of n is shown in the inset. (Reprinted from Ref. [113], with the permission of AIP Publishing)

henceforth $(n, n)^-$, and $V_nBz_{n-1}^-$ ($n = 2$–5), denoted as $(n, n-1)^-$. The EA for each cluster was obtained in the same manner as those for $(n, n+1)$ and plotted against n in Fig. 8.22. It can clearly be seen from the figure that, in the range of $n \geq 3$, the EAs for (n, n) and $(n, n-1)$ monotonically increased with increasing n and converged on the EA of $(n, n+1)$. Taken into account that the monotonic

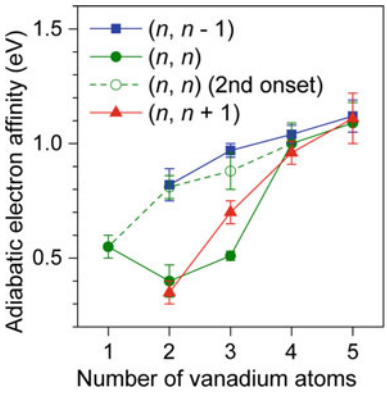

Fig. 8.22 Experimental EAs for V_nBz_m ($n = 1$–5, $m = n - 1$, n, and $n + 1$) as a function of n. The threshold energies of the second peaks in the PE spectra for V_2Bz_2 and V_3Bz_3 were determined by Gaussian fitting and are called the "second onset" and marked using open circles (°) connected with a dashed line. The connecting lines are provided to guide the eye. (Reprinted from Ref. [115], with the permission of AIP Publishing)

increase in the EA for $(n, n + 1)$ is attributable to the delocalized orbital along with the V atoms formation, EA would only be a function of n if the same number of V atoms were stacked alternately in a sandwich fashion. Indeed, similar AEAs were found for the clusters with $n = 4$ and 5 and different m values, thus suggesting that $(n, n - 1)^{0/-}$ and $(n, n)^{0/-}$ can also have one-dimensional sandwich structures with similar electronic configurations.

At $n = 1$–3, on the other hand, EA is dependent on both n and m. The non-monotonic variation in the EA between the (1, 1), (2, 2), and (3, 3) clusters was of particular interest because it implied that there may be structural isomers of these clusters. Figure 8.22 also indicates "second onsets" for (2, 2) and (3, 3), obtained by deconvoluting the PE spectra (for $(2, 2)^-$ shown in Fig. 8.23a, b) through a Gaussian fitting technique. Interestingly, the second onsets do not hint at possible excited states but at the presence of higher-lying isomers of the anions, as they disappeared under a different experimental (Bz-poor) condition (Fig. 8.23b). In fact, our DFT calculations found three and two isomers for (2, 2) and its anion, respectively, as displayed in Fig. 8.23c, d. The dimer sandwiches **1** and **4** have the lowest spin states, while the alternating sandwiches **2**, **3**, and **5** favor high-spin multiplicities that originate from the V atoms. Comparison between experimental and calculated EAs and VDEs assigned the first and second peaks, labeled (i) and (ii) in the PE spectrum of Fig. 8.23a, to **4** and **5**, respectively, showing the coexistence of the two isomers for $(2, 2)^-$. It is conceivable that, due to their "packed" structures, the non-alternating sandwich clusters such as **1** and **4** could limit their growth process, making alternating sandwiches major at larger n. The multiple-decker sandwich formation of $V_nBz_m{}^{0/-}$ regardless of $m = n + 1$, n, and $n - 1$ could extend its technological use because $V_nBz_{n+1}{}^{0/-}$ clusters do not lose their electronic and magnetic character via elimination/modification of their terminal Bz molecules.

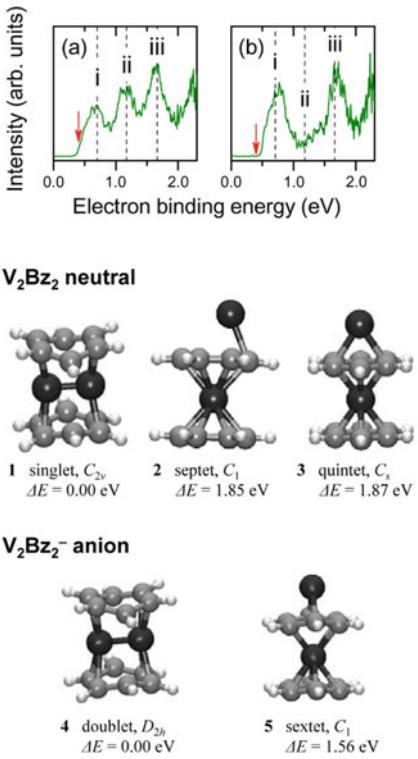

Fig. 8.23 (**a**, **b**) show PE spectra for $V_2Bz_2^-$ acquired using 532 nm radiation under relatively benzene-poor and benzene-rich conditions, respectively. The EBEs at the vertical arrows and the dashed lines (labeled *i–iii*) correspond with the experimental EAs and VDEs, respectively. The amount of Bz introduced into our apparatus could be qualitatively controlled by changing the pulse duration (by controlling the pulsed valve). (**c**, **d**) display low-lying isomers of the V_2Bz_2 and its anionic clusters, respectively, with their spin states, symmetries, and relative energies. (Reprinted from Ref. [115], with the permission of AIP Publishing)

8.3.5 *Multiple-Decker and Ring Sandwich Formation of Manganese-Benzene Cluster Anions*

In Sects. 8.3.3 and 8.3.4, we described our research on the electronic and magnetic characteristics of $V_nBz_m^{0/-}$ ($m = n - 1$, n, and $n + 1$) multiple-decker sandwich clusters. Our finding further motivates such characterization of multiple-decker sandwich clusters containing different metal atoms. Indeed, several theoreticians have predicted that an infinite Mn-Bz sandwich wire would have half metallicity that surpasses that of a V-Bz wire [96, 100]. However, several transition metals (M = Cr, Mn, and Cu) had never produced any larger clusters than mononuclear MBz_2 in the reaction with benzene, as stated in Sect. 8.3.3. Nevertheless, we reported a joint anion PES and theoretical study on $Mn_nBz_m^-$ cluster anions, hereafter denoted $(n, m)^-$ [116]. In this subsection, we unveil unprecedented structures and electromagnetic properties of $(n, n)^-$ cluster anions, which in turn are quite different from those predicted in the former studies [96, 100].

In order to produce $(n, m)^-$ anions, we used the same laser vaporization source as described in Sect. 8.3.4. Figure 8.24 shows the mass spectrum for produced anions, indicating that various $(n, m)^-$ anions were generated without dehydrogenation. It is understood that efficient cooling in clustering reactions led to the complete $(n, m)^-$

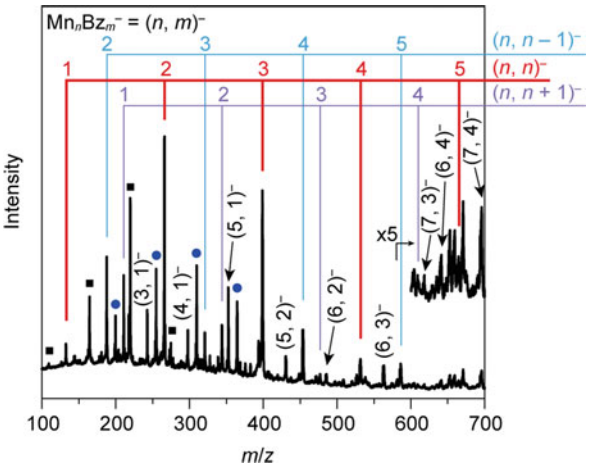

Fig. 8.24 Mass spectrum of $Mn_nBz_m^-$. The peak assignments for $(n, m)^- = (n, n-1)^-$, $(n, n)^-$, and $(n, n+1)^-$ are indicated with vertical lines. Several dominant $(n, m)^-$ clusters with $m \leq n-2$ are also labeled. Coexistent naked Mn_n^- clusters and incomplete Mn-Bz cluster anions are marked by ■ and •, respectively. (Reproduced from Ref. [116] with permission from the Royal Society of Chemistry)

formation, as we discussed for the case of $V_nBz_m^-$ clusters. Anion PE spectra taken for $(n, n)^-$ clusters (n = 1–5) are displayed in Fig. 8.25a. Our DFT calculations revealed unprecedented tilted sandwich structures for all $(n, n)^-$ studied (see **1**, **2a**, **3a**, **4**, and **5** in Fig. 8.25b) in contrast to linear sandwich chains assumed in the former studies [96, 100]. The PE spectra can be assigned to the tilted clusters though isomers **2b** and **3b** could also contribute to the spectra for n = 2 and 3, as were seen in the case of V_2Bz_2 and V_3Bz_3. Interestingly, the tilted form exhibits size evolution of its spin multiplicity that is even higher than that of $V_nBz_{n+1}^{0/-}$; for example, $Mn_5Bz_5^-$ (**5**) has a spin state of $2S + 1 = 17$, while multiple-decker $V_5Bz_6^-$ is a quartet. Such high-spin states of $Mn_nBz_n^-$ are accounted for by three unpair electrons (i.e., 1 dσ and 2 dπ electrons) in each Mn(η^6-Bz) unit that is further η^2-bound to each other in the structures of **3a**, **4**, and **5**.

The tilted sandwich structures of $Mn_nBz_n^-$ addressed another question whether or not the size evolution of the $Mn_nBz_n^-$ is terminated at the finite number n, in contrast to the linear V-Bz system. Indeed, a couple of ring-structured $Mn_{18}Bz_{18}^{-/0}$ were computationally anticipated as it was estimated from the extrapolation of the structures **3a**, **4**, and **5** that cyclization of $Mn_nBz_n^-$ occurs at n = 18. Our structure optimization of $Mn_{18}Bz_{18}$ starting from a C_{18h} geometry obtained a neutral structure with perfect C_{18h} symmetry, as shown in Fig. 8.26a, when assuming a spin state of $2S + 1 = 55$. This structure has a pretty large negative spin density ($\rho_s = -0.52$) for each Bz and the positive spin density of $\rho_s = 3.52$ per a Mn atom. Likewise, the anionic $Mn_{18}Bz_{18}^-$ was determined to be C_2 symmetric with a spin state of $2S + 1 = 54$. In both cases, the calculations on the neighboring spin states found higher energies or even met convergence problems within C_{18h} or C_2 symmetry. In fact, the spin state of the anionic $Mn_{18}Bz_{18}^-$ is well consistent with the extrapolation from those of $Mn_nBz_n^-$ (n = 1–5), as shown in Fig. 8.26b.

We further highlight the unique electromagnetic properties of $Mn_{18}Bz_{18}$ cluster. The valence orbitals in the majority (α) spin part of the neutral $Mn_{18}Bz_{18}$ are

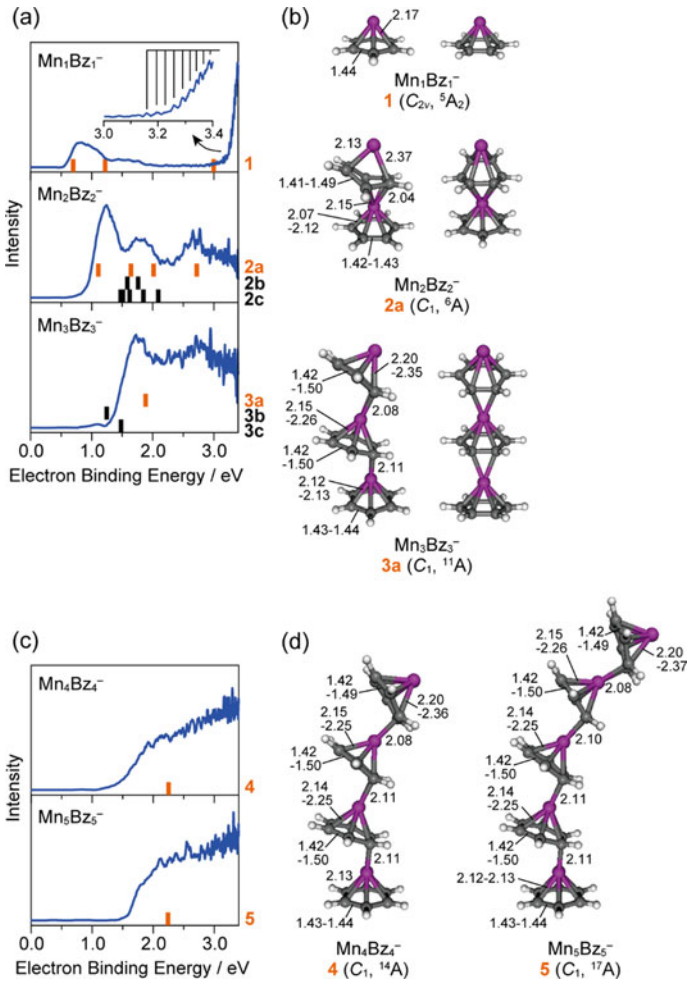

Fig. 8.25 (**a**) Anion PE spectra for $Mn_nBz_n^-$ ($n = 1$–5) taken with 355 nm (3.49 eV) radiation. The calculated VDEs of the plausible structures are indicated below the spectra with vertical bars. Bold-faced labels right to the VDE bars are denoted to identify the structures. (**b**) The most plausible structures for $Mn_nBz_n^-$ ($n = 1$–5) with their symmetries and electronic states. Typical bond lengths are indicated in Å. (Reproduced from Ref. [116] with permission from the Royal Society of Chemistry)

displayed in Fig. 8.27a. The α-HOMO has a delocalized bonding character and can be divided into contributions from the α-HOMOs of each quartet-state MnBz unit (inset of Fig. 8.27a). The degenerate α-HOMO – 1 and α-HOMO – 2, and other orbitals (6 sets of degenerate and 1 nondegenerate) with the α spin are isomorphous to the α-HOMO. Interestingly, each delocalized $Mn_{18}Bz_{18}$ orbital allows us to define the number of its orbital nodes k, analogously to π conjugated hydrocarbon

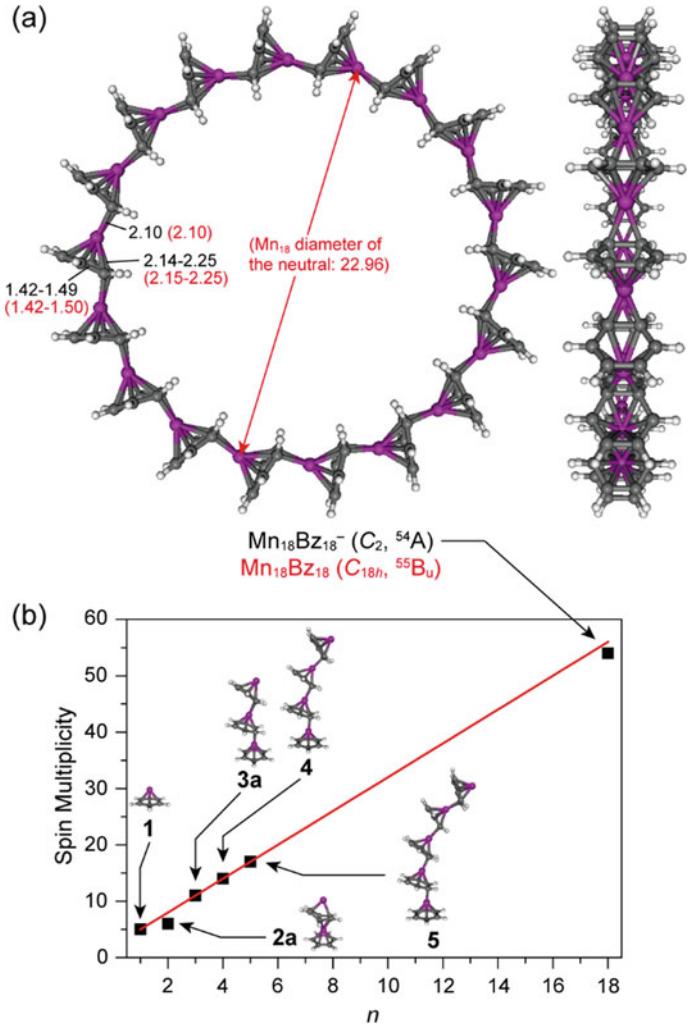

Fig. 8.26 (**a**) Top and side views of the optimized structures for $Mn_{18}Bz_{18}^{-/0}$ ring clusters with their symmetries and electronics states. Typical bond length are indicated in Å (those of the neutral are given in parentheses). (**b**) Side-dependent spin multiplicities of $Mn_nBz_n^-$ ($n = 1$–5 and 18). The linear extrapolation of the spin multiplicities for tilted multiple-decker sandwich structures is expressed by the red line. (Reproduced from Ref. [116] with permission from the Royal Society of Chemistry)

systems. Compared to [18]annulene ($C_{18}H_{18}$), which has an 18-membered ring structure with 18π electrons (Fig. 8.27b), particularly unusual for $Mn_{18}Bz_{18}$ is that the smaller number of nodes is rather associated with the energetically higher orbital.

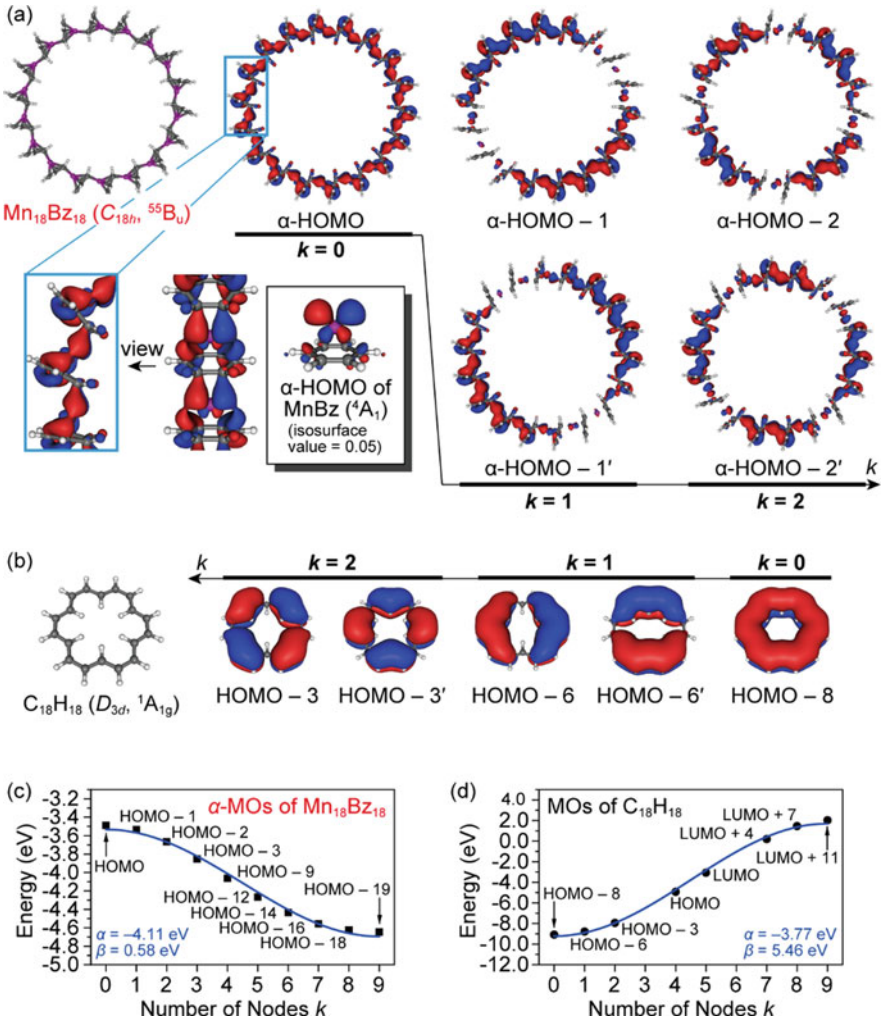

Fig. 8.27 (**a**) Valence orbital pictures in the majority (α) spin part of the neutral $Mn_{18}Bz_{18}$ cluster. The number of nodes k is given for each delocalized orbital. Inset shows top and side views of the partially magnified α-HOMO. The isosurface value of 0.01 was adopted unless otherwise noted. (**b**) Orbital pictures of [18]annulene ($C_{18}H_{18}$) with an isosurface value = 0.01, having the same k values as depicted in (**a**) for comparison. (**c**) Orbital energies plotted against k for the $Mn_{18}Bz_{18}$ α-HOMO and lower-lying isomorphous orbitals, and (**d**) those for the $C_{18}H_{18}$ orbitals composed of delocalized π electrons. Blue curves are obtained by a curve-fitting analysis using Eq. (8.1). (Reproduced from Ref. [116] with permission from the Royal Society of Chemistry)

For an intelligible explanation of such delocalized electron systems, we use a simple Hückel model: for cyclic conjugated systems, each molecular orbital energy ε_k is given as

$$\varepsilon_k = \alpha + 2\beta \cos\left(\frac{2\pi}{N}k\right) \qquad \left(0 \leq k \leq \frac{N}{2}\right) \tag{8.1}$$

where the Hückel parameters α and β are employed. The number of basis functions N is set to 18 in both cases of $Mn_{18}Bz_{18}$ and $C_{18}H_{18}$, in which fragment (or atomic) orbitals of each MnBz and C are treated, respectively. To apply this model, orbital energies were plotted against k and fit by Eq. (8.1); namely, the plots for the $Mn_{18}Bz_{18}$ α-HOMO and lower-lying isomorphous orbitals are shown in Fig. 8.27c. The same analysis was done for the $C_{18}H_{18}$ orbitals as plotted in Fig. 8.27d. From the figure, the simple Hückel model can describe the $Mn_{18}Bz_{18}$ plot but claims a positive β which contrasts the conventional cases (with a negative β) as demonstrated for $C_{18}H_{18}$. Taken into consideration that β in general is not significantly affected by two-electron repulsive interactions, the positive β of $Mn_{18}Bz_{18}$ may originate from its strong intra-atomic exchange interactions within the Mn $3d$ electrons. In fact, former studies [90, 111, 117] have explained that the intra-atomic exchange interactions within the metal $3d$ orbitals induce localized positive and negative spin densities on each metal atom and Bz molecule, respectively. The ferromagnetic spin ordering of multiple-decker V_nBz_{n+1} is stabilized by this spin localization, and that of $Mn_{18}Bzn_{18}{}^{-/0}$ may also be explained in the same manner. Although to date it has not been characterized experimentally, $Mn_{18}Bz_{18}$, having the planar (i.e., 2D) ring structure, could be exploited for applications in future nanoscale electronics and spintronics.

8.4 Conclusions and Outlook

In this chapter, we first wrote a brief history of organometallic sandwich complexes starting from the discovery of ferrocene. We then described enormous contributions on the gas-phase synthesis and spectroscopic characterization for transition metal sandwich complexes. Our particular focus among them was on the formation and electromagnetic properties of transition metal-benzene sandwich clusters. In the reaction with benzene, early transition metals (Sc, Ti, and V) form multiple-decker metal-benzene sandwich clusters, where metal atoms and benzene molecules are piled up alternately. This multiple-decker formation was confirmed by means of laser spectroscopies and quantum chemical calculations. The multiple-decker clusters of V_nBz_{n+1} exhibit a linear increase of their magnetic moment with increasing the cluster size. The interplay between anion photoelectron spectroscopy and theoretical calculations revealed that such magnetic behavior is attributed to the ferromagnetic spin ordering of $3d$ electrons localized at each metal atom. Interestingly, these unique structural and electronic features of V_nBz_{n+1} do not change either upon electron attachment which generates the corresponding anions ($V_nBz_{n+1}{}^-$) or, in case of $n \geq 4$, even upon elimination of a terminal benzene

molecule that yields $V_nBz_m^{0/-}$ ($m = n - 1$ and n). Furthermore, we described our recent research that studied a new family of manganese-benzene cluster anions, $Mn_nBz_n^-$, which were found to exhibit unprecedented multiple-decker structures with a tilted Mn-Bz stacking and a monotonically increasing behavior of their high-spin multiplicities.

Lastly, we herein refer to several studies that are aimed at the controlled assembly of transition metal-benzene sandwich clusters. For the functionalization of such clusters, a promising route is to assemble the clusters on surfaces with certain hierarchical nanostructures and tailored dimensionality. However, the fabrication of cluster-based assemblies on surfaces requires a deposition technique that allows clusters to be deposited softly onto a surface, as clusters may be dissociated upon impact. In addition, a deep understanding of the cluster-surface interaction is crucial because cluster structures are often perturbed by a strong interaction with surfaces. To this end, Judai et al. [60, 118] adopted a soft-landing technique to deposit VBz_2^+ cluster cations into a low-temperature Ar matrix with precise control of deposition energy. The Ar matrix was chosen as it is known to serve as a buffer dissipating the kinetic energy of the projectile clusters and keeping the cluster largely intact [119–120]. Nagaoka et al. later deposited VBz_2^+ [121], $V_2Bz_3^+$ [122], and $Cr(aniline)_2^+$ cations [123] onto alkanethiolate self-assembled monolayers (SAMs). Infrared reflection absorption spectroscopy (IRAS) confirmed that, on both the substrates, the deposited clusters are neutralized and maintain sandwich structures. While the use of Ar matrix is limited to cryogenic temperature conditions, SAMs can support the sandwich clusters even at room temperature. In addition, the sandwich clusters can be highly oriented on the SAMs. Very recently, Huttmann et al. [124] synthesized europium-cyclooctatetraene (Eu-COT) nanowires on a graphene substrate, where the nanowires are found to be lying parallel to each other. Scanning tunneling spectroscopy (STS) and low-temperature X-ray magnetic circular dichroism (XMCD) revealed that the Eu-COT wire is a ferromagnetic insulator [125]. These immobilization methods, together with spectroscopic applications and theoretical approaches, can readily provide a direct route to investigate the low-dimensional functionality of transition metal-benzene sandwich clusters on a substrate. As such, functionalized sandwich clusters will open up possibilities for exploiting themselves as new building blocks in future molecular electronics and spintronics.

Acknowledgments We are grateful to Prof. S. Yabushita (Keio University), Dr. T. Iwasa (Hokkaido University), and Prof. K. Kanoda (The University of Tokyo) for fruitful discussion. This work is partly supported by the program of Exploratory Research for Advanced Technology (ERATO) in Japan Science and Technology Agency (JST) entitled with "Nakajima Designer Nanocluster Assembly Project" and by JSPS KAKENHI of Grant-in-Aids for Scientific Research (A) Grant Number 15H02002. The computations were partly performed using Research Center for Computational Science, Okazaki, Japan.

References

1. R.P. Feynman, There's plenty of room at the bottom. Caltech Eng. Sci. **23**, 22–36 (1960)
2. R. Kubo, Electronic properties of metallic fine particles. I. J. Phys. Soc. Jpn. **17**, 975–986 (1962)
3. W.A. de Heer, The physics of simple metal clusters: Experimental aspects and simple models. Rev. Mod. Phys. **65**, 611–676 (1993)
4. B. von Issendorff, O. Cheshnovsky, Metal to insulator transitions in clusters. Annu. Rev. Phys. Chem. **56**, 549–580 (2005)
5. M. Brack, The physics of simple metal clusters: Self-consistent jellium model and semiclassical approaches. Rev. Mod. Phys. **65**, 677–732 (1993)
6. U. Heiz, U. Landman (eds.), *Nanocatalysis* (Springer, Berlin, 2007)
7. H. Haberland (ed.), *Clusters of Atoms and Molecules II: Solvation and Chemistry of Free Clusters, and Embedded, Supported and Compressed Clusters* (Springer, Berlin, 1994)
8. B.M. Smirnov, R.S. Berry, *Phase Transitions of Simple Systems* (Springer, Berlin, 2008)
9. M. Mitsui, A. Nakajima, Photoelectron Spectroscopy of Organic Clusters, in *Handbook of Nanophysics*, (CRC Press, Boca Raton, 2010)
10. R.H. Crabtree, *The Organometallic Chemistry of the Transition Metals*, 5th edn. (Wiley, Hoboken, 2016)
11. A. Nakajima, K. Kaya, A novel network structure of organometallic clusters in the gas phase. J. Phys. Chem. A **104**, 176–191 (2000)
12. T.J. Kealy, P.L. Pauson, A new type of organo-Iron compound. Nature **168**, 1039–1040 (1951)
13. G. Wilkinson, M. Rosenblum, M.C. Whiting, R.B. Woodward, The structure of iron Bis-cyclopentadienyl. J. Am. Chem. Soc. **74**, 2125–2126 (1952)
14. E.O. Fischer, W. Pfab, Cyclopentadien-Metallkomplexe, ein neuer Typ metallorganischer Verbindungen. Z. Naturforsch. B **7**, 377–379 (1952)
15. J.W. Lauher, R. Hoffmann, Structure and chemistry of bis(cyclopentadienyl)-MLn complexes. J. Am. Chem. Soc. **98**, 1729–1742 (1976)
16. E.O. Fischer, R. Jira, Di-cyclopentadienyl-kobalt(II). Z. Naturforsch. B **8**, 327–328 (1953)
17. E.O. Fischer, W. Hafner, Di-benzol-chrom. Z. Naturforsch. B **10**, 665–668 (1955)
18. A. Streitwieser, U. Müller-Westerhoff, Bis(cyclooctatetraeny1)uranium (Uranocene). A new class of sandwich complexes that utilize atomic f orbitals. J. Am. Chem. Soc. **90**, 7364 (1968)
19. N. Rösch, A. Streitwieser Jr., SCF-Xα scattered-wave MO study of thorocene and uranocene. J. Organomet. Chem. **145**, 195–200 (1978)
20. E.L. Muetterties, J.R. Bleeke, E.J. Wucherer, T. Albright, Structural, stereochemical, and electronic features of arene-metal complexes. Chem. Rev. **82**, 499–525 (1982)
21. E.O. Fischer, H.P. Kögler, Über Aromatenkomplexe von Metallen, IX. Di-Benzol-Vanadin(O). Chem. Ber. **90**, 250–255 (1957)
22. A. Salzer, H. Werner, A new route to triple-decker sandwich compounds. Angew. Chem. Int. Ed. **11**, 930–932 (1972)
23. W. Siebert, 2,3-Dihydro-1,3-diborole-metal complexes with activated C-H bonds: Building blocks for multilayered sandwich compounds. Angew. Chem. Int. Ed. **24**, 943–958 (1985)
24. H. Werner, New varieties of sandwich complexes. Angew. Chem. Int. Ed. **16**, 1–9 (1977)
25. M. Munakata, L.P. Wu, G.L. Ning, A new type of multilayer system–silver(I) complexes of polycyclic aromatic compounds. Coord. Chem. Rev. **198**, 171–203 (2000)
26. P.L. Timms, Chemistry of transition-metal vapours. Part I. reactions with trifluorophosphine and related compounds. J. Chem. Soc. A **1970**, 2526–2528 (1970)
27. P.S. Skell, L.D. Wescott, Chemical properties of C3, a dicarbene. J. Am. Chem. Soc. **85**, 1023–1023 (1963)
28. R. Middleton, J.R. Hull, S.R. Simpson, C.H. Tomlinson, P.L. Timms, Chemistry of transition-metal vapours. Part III. Formation of complexes with arenes, trifluorophosphine, and nitric oxide. J. Chem. Soc. Dalton Trans. **1**, 120–124 (1973)

29. P.L. Timms, R.B. King, Preparative applications of metal vapours obtained by evaporation of metal powders from coated filaments : A new preparation of dibenzene-ruthenium and observation of its limiting N.M.R. spectrum. J. Chem. Soc. Chem. Commun. **22**, 898–899 (1978)
30. W.M. Lamanna, Metal vapor synthesis of a novel triple-decker sandwich complex: (η_6-mesitylene)$_2$(μ-η_6:η_6-mesitylene)Cr_2. J. Am. Chem. Soc. **108**, 2096–2097 (1986)
31. R.E. Smalley, Laser studies of metal cluster beams. Laser Chem. **2**, 167–184 (1983)
32. P.M. Holland, A.W. Castleman, The thermochemical properties of gas-phase transition metal ion complexes. J. Chem. Phys. **76**, 4195–4206 (1982)
33. H. Higashide, T. Kaya, M. Kobayashi, H. Shinohara, H. Sato, Reactions of benzene clusters with metal ions as studied by the laser ablation—Molecular beam method: Observation of clustered complex ions $M(C_6H_6)_n^+$ ($n \geqslant 2$) and fragment complex ions $M(C_6H_6)(C_XH_Y)^+$ with $X \leqslant$ and $Y \leqslant 4$. Chem. Phys. Lett. **171**, 297–302 (1990)
34. C.S. Yeh, K.F. Willey, D.L. Robbins, J.S. Pilgrim, M.A. Duncan, Photodissociation spectroscopy of Mg^+H_2O. Chem. Phys. Lett. **196**, 233–238 (1992)
35. F. Misaizu, M. Sanekata, K. Fuke, S. Iwata, Photodissociation study on $Mg^+(H2O)_n$, n=1–5: Electronic structure and photoinduced intracluster reaction. J. Chem. Phys. **100**, 1161–1170 (1994)
36. K.F. Willey, P.Y. Cheng, K.D. Pearce, M.A. Duncan, Photoinitiated charge transfer and dissociation in mass-selected metalloorganic complexes. J. Phys. Chem. **94**, 4769–4772 (1990)
37. Y.-M. Chen, P.B. Armentrout, Collision-induced dissociation of $Ag(C_6H_6)^+$. Chem. Phys. Lett. **210**, 123–128 (1993)
38. F. Meyer, F.A. Khan, P.B. Armentrout, Thermochemistry of transition metal benzene complexes: Binding energies of $M(C_6H_6)x^+$ ($x = 1, 2$) for M = Ti to Cu. J. Am. Chem. Soc. **117**, 9740–9748 (1995)
39. S. Maruyama, L.R. Anderson, R.E. Smalley, Direct injection supersonic cluster beam source for FT-ICR studies of clusters. Rev. Sci. Instrum. **61**, 3686–3693 (1990)
40. P. Milani, W.A. de Heer, Improved pulsed laser vaporization source for production of intense beams of neutral and ionized clusters. Rev. Sci. Instrum. **61**, 1835–1838 (1990)
41. A. Nakajima, T. Kishi, T. Sugioka, Y. Sone, K. Kaya, Mass distributions of aluminum negative cluster ions and their binary cluster ions mixed with a carbon atom. Chem. Phys. Lett. **177**, 297–300 (1991)
42. S. Nonose, Y. Sone, K. Onodera, S. Sudo, K. Kaya, Structure and reactivity of bimetallic cobalt-vanadium (Co_nV_m) clusters. J. Phys. Chem. **94**, 2744–2746 (1990)
43. K. Hoshino, T. Kurikawa, H. Takeda, A. Nakajima, K. Kaya, Structures and ionization energies of sandwich clusters (V_n(benzene)$_m$). J. Phys. Chem. **99**, 3053–3055 (1995)
44. P. Weis, P.R. Kemper, M.T. Bowers, Structures and energetics of $V_n(C_6H_6)_m^+$ clusters: Evidence for a quintuple-decker sandwich. J. Phys. Chem. A **101**, 8207–8213 (1997)
45. A. Nakajima, Study on electronic properties of composite clusters toward nanoscale functional advanced materials. Bull. Chem. Soc. Jpn. **86**, 414–437 (2013)
46. T. Kurikawa, M. Hirano, H. Takeda, K. Yagi, K. Hoshino, A. Nakajima, K. Kaya, Structures and ionization energies of cobalt-benzene clusters (Co_n(benzene)$_m$). J. Phys. Chem. **99**, 16248–16252 (1995)
47. T. Kurikawa, H. Takeda, A. Nakajima, K. Kaya, Structures and stabilities of 3d-transition metal-benzene organometallic clusters. Z. Phys. D **40**, 65–69 (1997)
48. T. Kurikawa, H. Takeda, M. Hirano, K. Judai, T. Arita, S. Nagao, A. Nakajima, K. Kaya, Electronic properties of organometallic metal−benzene complexes [M_n(benzene)$_m$ (M = Sc−Cu)]. Organometallics **18**, 1430–1438 (1999)
49. Y. Huang, B.S. Freiser, Synthesis of Bis(buckminsterful1erene)nickel cation, $Ni(C_{60})_2^+$, in the gas phase. J. Am. Chem. Soc. **113**, 8186–8187 (1991)
50. Y. Basir, S.L. Anderson, Interaction of Mn^+ and Mn_2^+ with C_{60}. Exohedral and endohedral metal-fullerene bonding. Chem. Phys. Lett. **243**, 45–48 (1995)

51. A. Nakajima, S. Nagao, H. Takeda, T. Kurikawa, K. Kaya, Multiple dumbbell structures of vanadium–C_{60} clusters. J. Chem. Phys. **107**, 6491–6494 (1997)
52. T. Kurikawa, S. Nagao, K. Miyajima, A. Nakajima, K. Kaya, Formation of cobalt-C_{60} clusters: Tricapped $Co(C_{60})_3$ unit. J. Phys. Chem. A **102**, 1743–1747 (1998)
53. S. Nagao, T. Kurikawa, K. Miyajima, A. Nakajima, K. Kaya, Formation and structures of transition metal-C_{60} clusters. J. Phys. Chem. A **102**, 4495–4500 (1998)
54. B.P. Pozniak, R.C. Dunbar, Monomer and dimer complexes of coronene with atomic ions. J. Am. Chem. Soc. **119**, 10439–10445 (1997)
55. J.W. Buchanan, J.E. Reddic, G.A. Grieves, M.A. Duncan, Metal and multimetal complexes with polyaromatic hydrocarbons: Formation and photodissociation of Fe_x-$(Coronene)_y$ cations. J. Phys. Chem. A **102**, 6390–6394 (1998)
56. J.W. Buchanan, G.A. Grieves, J.E. Reddic, M.A. Duncan, Novel mixed ligand sandwich complexes: Competitive binding of iron with benzene, coronene, and C_{60}. Int. J. Mass Spectrom. **182–183**, 323–333 (1999)
57. N.R. Foster, G.A. Grieves, J.W. Buchanan, N.D. Flynn, M.A. Duncan, Growth and photodissociation of Cr_x-$(Coronene)_y$ complexes. J. Phys. Chem. A **104**, 11055–11062 (2000)
58. M.A. Duncan, A.M. Knight, Y. Negishi, S. Nagao, K. Judai, A. Nakajima, K. Kaya, Photoelectron spectroscopy of $V_x(Coronene)_y$ and $Ti_x(Coronene)_y$ anions. J. Phys. Chem. A **105**(44), 10093–10097 (2001)
59. M. Hirano, K. Judai, A. Nakajima, K. Kaya, Effect of ring substituents on formation rates for vanadium-arene clusters. J. Phys. Chem. A **101**, 4893–4899 (1997)
60. K. Judai, M. Hirano, H. Kawamata, S. Yabushita, A. Nakajima, K. Kaya, Formation of vanadium-arene complex anions and their photoelectron spectroscopy. Chem. Phys. Lett. **270**, 23–30 (1997)
61. K. Judai, Y. Nakamura, M. Tachibana, Y. Negishi, A. Nakajima, K. Kaya, Photoelectron spectroscopy of scandium-arene complex anions. Chem. Lett. **30**, 114–115 (2001)
62. T. Yasuike, A. Nakajima, S. Yabushita, K. Kaya, Why do vanadium atoms form multiple-decker sandwich clusters with benzene molecules efficiently? J. Phys. Chem. A **101**, 5360–5367 (1997)
63. P.B. Armentrout, Electronic state-specific transition metal ion chemistry. Annu. Rev. Phys. Chem. **41**, 313–344 (1990)
64. C.E. Moore, *Atomic Energy Levels* (National Bureau of Standards, Washington, DC, 1949)
65. J. Hu, T.W. Odom, C.M. Lieber, Chemistry and physics in one dimension: Synthesis and properties of nanowires and nanotubes. Acc. Chem. Res. **32**, 435–445 (1999)
66. J.W. Mintmire, B.I. Dunlap, C.T. White, Are fullereue tubules metallic? Phys. Rev. Lett. **68**, 631–634 (1992)
67. R. Saito, M. Fujita, G. Dresselhaus, M.S. Dresselhaus, Electronic structure of chiral graphene tubules. Appl. Phys. Lett. **60**, 2204–2206 (1992)
68. J.W.G. Wildöer, L.C. Venema, A.G. Rinzler, R.E. Smalley, C. Dekker, Electronic structure of atomically resolved carbon nanotubes. Nature **391**, 59–62 (1998)
69. D. Gatteschi, R. Sessoli, J. Villain, *Molecular Nanomagnets* (Oxford University Press, New York, 2006)
70. G.S. Papaefstathiou, A. Escuer, C.P. Raptopoulou, A. Terzis, S.P. Perlepes, R. Vicente, Defective double-cubane, tetranuclear manganese (II) and cobalt (II) complexes with simultaneous $\mu_{1,1}$-azido and μ-O bridges. Eur. J. Inorg. Chem. **6**, 1567–1574 (2001)
71. C. Dendrinou-Samara, M. Alexiou, C.M. Zaleski, J.W. Kampf, M.L. Kirk, D.P. Kessissoglou, V.L. Pecoraro, Synthesis and magnetic properties of a metallacryptate that behaves as a single-molecule magnet. Angew. Chem. Int. Ed. **42**, 3763–3766 (2003)
72. D.E. Freedman, W.H. Harman, T.D. Harris, G.J. Long, C.J. Chang, J.R. Long, Slow magnetic relaxation in a high-spin iron(II) complex. J. Am. Chem. Soc. **132**, 1224–1225 (2010)
73. F. Habib, O.R. Luca, V. Vieru, M. Shiddiq, I. Korobkov, S.I. Gorelsky, M.K. Takase, L.F. Chibotaru, S. Hill, R.H. Crabtree, M. Murugesu, Influence of the ligand field on slow magnetization relaxation versus spin crossover in mononuclear cobalt complexes. Angew. Chem. Int. Ed. **52**, 11290–11293 (2013)

74. R. Clérac, H. Miyasaka, M. Yamashita, C. Coulon, Evidence for single-chain magnet behavior in a Mn^{III}-Ni^{II} chain designed with high spin magnetic units: A route to high temperature metastable magnets. J. Am. Chem. Soc. **124**, 12837–12844 (2002)
75. W.-X. Zhang, R. Ishikawa, B. Breedlove, M. Yamashita, Single-chain magnets: Beyond the Glauber model. RSC Adv. **3**, 3772–3798 (2013)
76. R.H. Baughman, A.A. Zakhidov, W.A. de Heer, Carbon nanotubes—The route toward applications. Science **297**, 787–792 (2002)
77. M.H. Jo, J.E. Grose, K. Baheti, M.M. Deshmukh, J.J. Sokol, E.M. Rumberger, D.N. Hendrickson, J.R. Long, H. Park, D.C. Ralph, Signatures of molecular magnetism in single-molecule transport spectroscopy. Nano Lett. **6**, 2014–2020 (2006)
78. L. Bogani, W. Wernsdorfer, Molecular spintronics using single-molecule magnets. Nat. Mater. **7**, 179–186 (2008)
79. L. Ma, A.H.C. Hart, S. Ozden, R. Vajtaia, P.M. Ajayan, Spiers memorial lecture advances of carbon nanomaterials. Faraday Discuss. **173**, 9–46 (2014)
80. S.N. Khanna, P. Jena, Assembling crystals from clusters. Phys. Rev. Lett. **69**, 1664–1667 (1993)
81. S.A. Claridge, A.W. Castleman Jr., S.N. Khanna, C.B. Murray, A. Sen, P.S. Weiss, Cluster-assembled materials. ACS Nano **3**, 244–255 (2009)
82. P. Gambardella, S. Rusponi, M. Veronese, S.S. Dhesi, C. Grazioli, A. Dallmeyer, I. Cabria, R. Zeller, P.H. Dederichs, K. Kern, C. Carbone, H. Brune, Giant magnetic anisotropy of single cobalt atoms and nanoparticles. Science **300**, 1130–1133 (2003)
83. R. Pandey, B.K. Rao, P. Jena, J.M. Newsam, Unique magnetic signature of transition metal atoms supported on benzene. Chem. Phys. Lett. **321**, 142–150 (2000)
84. R. Pandey, B.K. Rao, P. Jena, M.A. Blanco, Electronic structure and properties of transition metal-benzene complexes. J. Am. Chem. Soc. **123**, 3799–3808 (2001)
85. C. Elschenbroich, E. Schmidt, R. Gondrum, B. Metz, O. Burghaus, W. Massa, S. Wocadlo, Metal π complexes of benzene derivatives. Germanium in the periphery of Bis(benzene)vanadium and Bis(benzene)chromium. Synthesis and structure of new heteram-etallocyclophanes. Organometallics **16**, 4589–4596 (1997)
86. J.M. Frost, K.L.M. Harriman, M. Murugesu, The rise of 3-d single-ion magnets in molecular magnetism: Towards materials from molecules? Chem. Sci. **7**, 2470–2491 (2016)
87. W. Gerlach, O. Stern, Das magnetische Moment des Silberatoms. Z. Phys. A **9**, 353–355 (1922)
88. K. Miyajima, A. Nakajima, S. Yabushita, M.B. Knickelbein, K. Kaya, Ferromagnetism in one-dimensional vanadium-benzene sandwich clusters. J. Am. Chem. Soc. **126**, 13202–13203 (2004)
89. K. Miyajima, M.B. Knickelbein, A. Nakajima, Stern-Gerlach studies of organometallic sandwich clusters. Eur. Phys. J. D. **34**, 177–182 (2005)
90. K. Miyajima, S. Yabushita, M.B. Knickelbein, A. Nakajima, Stern-Gerlach experiments of one-dimensional metal-benzene sandwich clusters: $M_n(C_6H_6)_m$ (M = Al, Sc, Ti, and V). J. Am. Chem. Soc. **129**, 8473–8480 (2007)
91. M.B. Knickelbein, Magnetic moments of bare and benzene-capped cobalt clusters. J. Chem. Phys. **125**, 044308-1–044308-7 (2006)
92. A.K. Kandalam, B.K. Rao, P. Jena, R. Pandey, Geometry and electronic structure of $V_n(Bz)_m$ complexes. J. Chem. Phys. **120**, 10414–10422 (2004)
93. J. Wang, P.H. Acioli, J. Jellinek, Structure and magnetism of V_nBz_{n+1} sandwich clusters. J. Am. Chem. Soc. **127**, 2812–2813 (2005)
94. X. Zhang, J. Wang, Structural, electronic, and magnetic properties of Co_n(benzene)$_m$ complexes. J. Phys. Chem. A **112**, 296–304 (2008)
95. M.M. Rahman, H. Kasai, E.S. Dy, Theoretical investigation of electric and magnetic properties of benzene–vanadium sandwich complex chain. Jpn. J. Appl. Phys. **44**, 7954–7956 (2005)
96. H. Xiang, J. Yang, J.G. Hou, Q. Zhu, One-dimensional transition metal−benzene sandwich polymers: Possible ideal conductors for spin transport. J. Am. Chem. Soc. **128**, 2310–2314 (2006)

97. V.V. Maslyuk, A. Bagrets, V. Meded, A. Arnold, F. Evers, M. Brandbyge, T. Bredow, I. Mertig, Organometallic benzene-vanadium wire: A one-dimensional half-metallic ferromagnet. Phys. Rev. Lett. **97**, 097201-1–097201-4 (2006)
98. Y. Mokrousov, N. Atodiresei, G. Bihlmayer, S. Heinze, S. Blügel, The interplay of structure and spin-orbit strength in the magnetism of metal-benzene sandwiches: From single molecules to infinite wires. Nanotechnology **18**, 495402-1–495402-12 (2007)
99. H. Weng, T. Ozaki, K. Terakura, Theoretical analysis of magnetic coupling in sandwich clusters $V_n(C_6H_6)_{n+1}$. J. Phys. Soc. Jpn. **77**, 014301-1–014301-9 (2007)
100. L. Shen, S.-W. Yang, M.-F. Ng, V. Ligatchev, L. Zhou, Y. Feng, Charge-transfer-based mechanism for half-metallicity and ferromagnetism in one-dimensional organometallic sandwich molecular wires. J. Am. Chem. Soc. **130**, 13956–13960 (2008)
101. L. Zhou, S.-W. Yang, M.-F. Ng, M.B. Sullivan, V.B.C. Tan, L. Shen, One-dimensional iron−cyclopentadienyl sandwich molecular wire with half metallic, negative differential resistance and high-spin filter efficiency properties. J. Am. Chem. Soc. **130**, 4023–4027 (2008)
102. L. Wang, Z. Cai, J. Wang, J. Lu, G. Luo, L. Lai, J. Zhou, R. Qin, Z. Gao, D. Yu, G. Li, W.N. Mei, S. Sanvito, Novel one-dimensional organometallic half metals: Vanadium-cyclopentadienyl, vanadium-cyclopentadienyl-benzene, and vanadium-anthracene wires. Nano Lett. **8**, 3640–3644 (2008)
103. X. Zhang, M.-F. Ng, Y. Wang, J. Wang, S.-W. Yang, Theoretical studies on structural, magnetic, and spintronic characteristics of sandwiched Eu_nCOT_{n+1} (n = 1-4) clusters. ACS Nano **3**, 2515–2522 (2009)
104. X. Zhang, Z. Tian, S.-W. Yang, J. Wang, Magnetic manipulation and half-metal prediction of one-dimensional bimetallic organic sandwich molecular wires $[CpTM_1CpTM_2]_\infty$ (TM_1 = Ti, Cr, Fe; TM_2 = Sc−Co). J. Phys. Chem. C **115**, 2948–2953 (2011)
105. X. Zhang, J. Han, Y. Liu, J. Wang, Structural, electronic, and magnetic properties of one-dimensional organic bimetal-naphthalene sandwich nanowires. J. Phys. Chem. C **116**, 5414–5419 (2012)
106. L. Horváthová, M. Dubecký, L. Mitas, I. Štich, Spin multiplicity and symmetry breaking in vanadium-benzene complexes. Phys. Rev. Lett. **109**, 053001-1–053001-5 (2012)
107. K.P. Kepp, Consistent descriptions of metal–ligand bonds and spin-crossover in inorganic chemistry. Coord. Chem. Rev. **257**, 196–209 (2013)
108. M. Kepenekian, J.-P. Gauyacq, N. Lorente, Difficulties in the ab initio description of electron transport through spin filters. J. Phys. Condens. Matter **26**, 104203-1–104203-8 (2014)
109. L. Horváthová, R. Derian, L. Mitas, I. Štich, Quantum Monte Carlo study of one-dimensional transition-metal organometallic cluster systems and their suitability as spin filter. Phys. Rev. B Condens. Matter **90**, 115414-1–115414-5 (2014)
110. K. Miyajima, K. Muraoka, M. Hashimoto, T. Yasuike, S. Yabushita, A. Nakajima, K. Kaya, Quasi-band electronic structure of V_n(benzene)$_{n+1}$ clusters. J. Phys. Chem. A **106**, 10777–10781 (2002)
111. T. Yasuike, S. Yabushita, Ionization energies and bonding scheme of multiple-decker sandwich clusters: $M_n(C_6H_6)_{n+1}$. J. Phys. Chem. A **103**, 4533–4542 (1999)
112. M.R. Zakin, D.M. Cox, R.O. Brickman, A. Kaldor, Benzene C-D bond activation by free vanadium cluster cations. J. Phys. Chem. **93**, 6823–6827 (1989)
113. T. Masubuchi, K. Ohi, T. Iwasa, A. Nakajima, Experimental and theoretical studies on the electronic properties of vanadium-benzene sandwich cluster anions, $V_nBz_{n+1}^-$ (n = 1-5). J. Chem. Phys. **137**, 224305-1–224305-9 (2012)
114. U. Even, J. Jortner, D. Noy, N. Lavie, C. Cossart-Magos, Cooling of large molecules below 1 K and He clusters formation. J. Chem. Phys. **112**, 8068–8071 (2000)
115. T. Masubuchi, T. Iwasa, A. Nakajima, Experimental and theoretical studies of the structural and electronic properties of vanadium–benzene sandwich clusters and their anions: $V_nBz_n^{0/-}$ (n = 1–5) and $V_nBz_{n-1}^{0/-}$ (n = 2–5). J. Chem. Phys. **141**, 214304-1–214304-8 (2014)
116. T. Masubuchi, T. Iwasa, A. Nakajima, Multiple-decker and ring sandwich formation of manganese–benzene organometallic cluster anions: $Mn_nBz_n^-$ (n = 1–5 and 18). Phys. Chem. Chem. Phys. **18**, 26049–26056 (2016)

117. A. Goto, S. Yabushita, Theoretical study on the spin states and intra-cluster spin relaxation of the one-dimensional metal–benzene sandwich clusters: $M_2(C_6H_6)_3$ (M = Sc, Ti, V). Chem. Phys. Lett. **454**, 382–386 (2008)
118. K. Judai, K. Sera, S.-i. Amatsutsumi, K. Yagi, T. Yasuike, S. Yabushita, A. Nakajima, K. Kaya, A soft-landing experiment on organometallic cluster ions: Infrared spectroscopy of V(benzene)$_2$ in Ar matrix. Chem. Phys. Lett. **334**, 277–284 (2001)
119. H.-P. Cheng, U. Landman, Controlled deposition, soft landing, and glass formation in nanocluster-surface collisions. Science **260**, 1304–1307 (1993)
120. K. Bromann, C. Félix, H. Brune, W. Harbich, R. Monot, J. Buttet, K. Kern, Controlled deposition of size-selected silver nanoclusters. Science **274**, 956–958 (1996)
121. S. Nagaoka, T. Matsumoto, E. Okada, M. Mitsui, A. Nakajima, Room-temperature isolation of V(benzene)$_2$ sandwich clusters via soft-landing into *n*-Alkanethiol self-assembled monolayers. J. Phys. Chem. B **110**, 16008–16017 (2006)
122. S. Nagaoka, T. Matsumoto, K. Ikemoto, M. Mitsui, A. Nakajima, Soft-landing isolation of multidecker V_2(benzene)$_3$ complexes in an organic monolayer matrix: An infrared spectroscopy and thermal desorption study. J. Am. Chem. Soc. **129**, 1528–1529 (2007)
123. S. Nagaoka, K. Ikemoto, K. Horiuchi, A. Nakajima, Soft- and reactive-landing of Cr(aniline)$_2$ sandwich complexes onto self-assembled monolayers: Separation between functional and binding sites. J. Am. Chem. Soc. **133**, 18719–18727 (2011)
124. F. Huttmann, N. Schleheck, N. Atodiresei, T. Michely, On-surface synthesis of sandwich molecular nanowires on graphene. J. Am. Chem. Soc. **139**, 9895–9900 (2017)
125. F. Huttmann, N. Rothenbach, S. Kraus, K. Ollefs, L.M. Arruda, M. Bernien, D. Thonig, A. Delin, J. Fransson, K. Kummer, N.B. Brookes, O. Eriksson, W. Kuch, T. Michely, H. Wende, Europium cyclooctatetraene nanowire carpets: A low-dimensional, organometallic, and ferromagnetic insulator. J. Phys. Chem. Lett. **10**, 911–917 (2019)